

Similarity of Neural Architectures Based on Input Gradient Transferability

Jaehui Hwang^{1,†} Dongyoon Han² Byeongho Heo² Song Park²
Sanghyuk Chun^{2,*} Jong-Seok Lee^{1,*}

¹ School of Integrated Technology, Yonsei University

² Naver AI Lab

[†] Works done while doing an internship at NAVER AI Lab.

^{*} Corresponding authors

Abstract

In recent years, a huge amount of deep neural architectures have been developed for image classification. It remains curious whether these models are similar or different and what factors contribute to their similarities or differences. To address this question, we aim to design a quantitative and scalable similarity function between neural architectures. We utilize adversarial attack transferability, which has information related to input gradients and decision boundaries that are widely used to understand model behaviors. We conduct a large-scale analysis on 69 state-of-the-art ImageNet classifiers using our proposed similarity function to answer the question. Moreover, we observe neural architecture-related phenomena using model similarity that model diversity can lead to better performance on model ensembles and knowledge distillation under specific conditions. Our results provide insights into why the development of diverse neural architectures with distinct components is necessary.

1. Introduction

The last couple of decades have seen the great success of deep neural networks (DNNs) in real-world applications, *e.g.*, image classification [39] and natural language processing [94]. The advances in the DNN architecture design have taken a key role in this success by making the learning process easier (*e.g.*, normalization methods [2, 46, 101] or skip connection [39]), enforcing human inductive bias in the architecture (*e.g.*, convolutional neural networks (CNNs) [52, 76]), or increasing model capability with the self-attention mechanism (*e.g.*, Transformers [94]). With different architectural components containing architectural design principles and elements, a number of different neural architectures have been proposed. They have different accuracies, but several researches [62] have pointed out that their predictions are not significantly different.

By this, can we say that recently developed DNN models with different architectural components are similar or the same? The answer is no. Existing studies have found differences by focusing on dissecting each network component layer-by-layer [50, 70] or providing a high-level understanding by visualization of loss surface [25], input gradient [77, 79], or decision boundary [78]. But similarity comparison methods from most of these studies are insufficient for facilitating comprehensive studies because they do not satisfy two criteria that widely applicable metrics should meet: (1) providing a quantitative similarity score and (2) being compatible with different base architectures (*e.g.*, CNN and Transformer). Recently, Sompalli *et al.* [78] suggested a similarity metric based on the on-manifold decision boundary using three images from different classes. However, this method needs heavy computation due to the triplet sampling process when the number of classes becomes large (*e.g.*, ImageNet [72] with 1,000 classes). If we limit the total computations, this method will suffer from inaccurate approximation with high variance.

In this paper, we aim to define a quantitative similarity function that is scalable and easily applicable to diverse architectures. We focus on the adversarial attack transferability, which can be a reliable approximation for comparing the input gradients, a widely-used framework to understand model behavior and difference between models, *e.g.*, how a model will change predictions by local pixel changes [3, 15, 75, 77, 79, 82, 83] and decision boundary [78]. As adversarial examples are generally generated based on input gradients [21, 32, 61], the similarity of adversarial examples will be highly related to the similarity of input gradients. Furthermore, the transferability of an adversarial sample indicates whether the decision boundaries at that point are similar or dissimilar.

Using the similarity function, we measure the pairwise attack transferability-based network similarity of 69 different neural architectures trained on ImageNet [72], provided by [99]. With the results of the similarity of 69 architectures, we analyze what components among 13 architectural com-

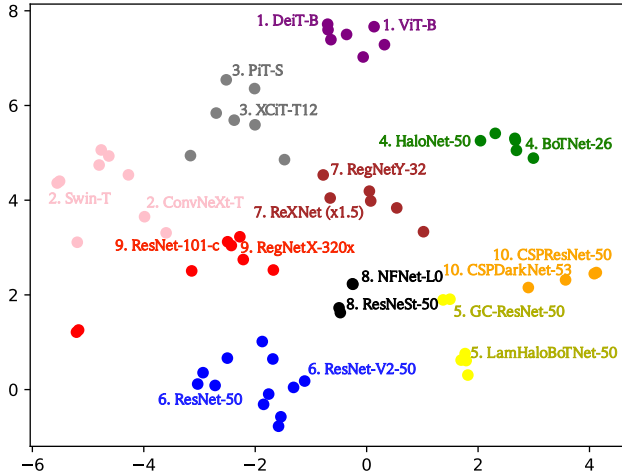


Figure 1: t-SNE plot showing ten clusters of 69 neural networks using the proposed similarity function. We cluster 69 neural networks in ten groups based on our proposed similarity function. The group number follows one of Tab. 3. Due to the space limit, we only illustrate representative models in each group.

ponents (*e.g.*, normalization, activation, the design choice for stem layers) that consist of neural architectures largely affect model diversity by gradient boosting regression and clustering on model similarities. Furthermore, we observe relationships between model similarity and model ensemble performances, and distillation performances. The main contributions of this work can be summarized as follows.

- We propose a novel similarity function that utilizes attack transferability, which provides a quantitative measure and is scalable across different neural architectures. Utilizing attack transferability offers several advantages that it is easy to conduct and reports stable results even when there is a change in data sampling.
- We conduct a comprehensive analysis using 69 models to investigate what components make neural architectures behave similarly or differently. To the best of our knowledge, this is the first large-scale analysis exploring the relationship between model similarity and architectural components. Furthermore, our findings are not limited to architectural components but also encompass training strategies. We find that different training strategies do not affect model diversity as much as architectural differences.
- We identify several outgrowths using our similarity based on adversarial attack transferability. First, we find model differences lead to better ensemble performance and analyze the reasons behind this. Additionally, we suggest new guidelines for selecting a teacher model suited to the student model in knowledge distillation [43]. These observations provide insights into why we need to develop diverse architectures.

2. Related work

In recent years, researchers have explored a **similarity between DNNs**. Several studies focused on comparing intermediate features [50, 70] for understanding the behavior of neural networks. By layer-by-layer comparison, they observed differences between layers, training methods, and architectures (*e.g.*, CNN and ViT). Other studies [25, 56, 66] have focused on loss landscapes, which helps to visualize the loss of models on the parameter space. However, these methods are limited to comparing models and observe overall model differences because they focus on model components and do not support quantitative measurement.

There also has been another line of research based on **prediction-based statistics**, *e.g.*, comparing the wrong and correct predictions [30, 31, 53, 73]. But just focusing on prediction values could be misleading because recent DNNs are getting almost perfect (*e.g.*, 100%) as they are getting more complex. Meding *et al.* [62] observed that recent DNNs show highly similar predictions. In this case, prediction-based methods will be no more informative.

Input gradient is another widely-used framework to understand model behavior, *e.g.*, how a model will change predictions by local pixel changes [3, 15, 75, 77, 79, 82, 83]. If two models are similar, their input gradients will also be similar. An input gradient-based method has several advantages; it is computationally efficient, and no additional training is required; it can provide a visual understanding of the given input. Usually, an input gradient-based quantity measures how the input gradient of a model matches the actual foreground [15], *i.e.*, it usually measures how a model explains the input well. However, due to the noise inherent in input gradients, directly measuring the difference between input gradients can be challenging.

Comparing the decision boundaries of two models will provide a high-level understanding of how two models behave differently for input changes and how models extract features from complicated data dimensions. In [78], the authors tried to analyze features of models by comparing their decision boundaries on the on-manifold plane containing picked three images. However, we observe that this approach derives unstable measurements on huge datasets (*e.g.*, ImageNet [72]) and is expensive (Sec. 3).

3. Network similarity function by input gradient transferability

In this section, we propose a quantitative similarity measure between two networks. We utilize adversarial attack transferability, which captures input gradients and decision boundary information. The attack transferability indicates whether an adversarial sample from a model can fool another model or not. The attack transferability can be a good approximation of measuring the differences in input gradi-

ents or model decision boundaries between models.

Input gradient is a popular way to understand model behavior, such as how a model will change predictions by local pixel changes. Our motivation is that if two models are more similar, the input gradients get more similar. However, because the input gradient is very noisy, directly measuring the difference between input gradients is also very noisy. Instead, we generate adversarial samples using gradient-based adversarial attacks (e.g., PGD [61], AutoAttack [21]). Because adversarial samples are updated by input gradients, adversarial samples will be similar if input gradients of two networks are similar. Therefore, we expect that high adversarial attack transferability denotes that two networks have similar input gradients.

Decision boundaries of models, which provide how models behave for the changes of input, are widely utilized to understand models. Our work is motivated by the idea that more similar models should have more similar decision boundaries. Measuring adversarial attack transferability is a good approximation of measuring the difference between model decision boundaries [49]. Specifically, if two models have similar decision boundaries, then the adversarial samples will be transferred (*i.e.*, will have high adversarial attack transferability); if two models have dissimilar decision boundaries, then the adversarial samples will not be transferred (see Fig. 2).

We propose a new similarity function that utilizes attack transferability, providing a reliable, easy-to-conduct, and scalable method for measuring the similarity between neural architectures. Formally, we generate adversarial samples x_A and x_B of model A and B for the given input x . Then, we measure the accuracy of model A using the adversarial sample for model B (called $\text{acc}_{B \rightarrow A}$). If A and B are the same, then $\text{acc}_{B \rightarrow A}$ will be zero (for simplicity, here, we may assume that the adversary can fool a model perfectly). On the other hand, if the input gradients of A and B differ significantly, then the performance drop will be neglectable because the adversarial sample is almost similar to the original image (*i.e.*, $\|x - x_B\| \leq \varepsilon$). Let X_{AB} be the set of inputs where both A and B predict correctly, y be the ground truth label, and $\mathbb{I}(\cdot)$ be the indicator function. We measure the similarity between two different models by:

$$s(A, B) = \log \left[\max \left\{ \varepsilon_s, 100 \times \frac{1}{2|X_{AB}|} \sum_{x \in X_{AB}} \{ \mathbb{I}(A(x_B) \neq y) + \mathbb{I}(B(x_A) \neq y) \} \right\} \right], \quad (1)$$

where ε_s is a small scalar value to prevent the ill-posedness of $s(\cdot)$. If $A = B$ and we have an oracle adversary, then $s(A, A) = \log 100$. In practice, a strong adversary (*e.g.*, PGD [61] or AutoAttack [21]) can easily achieve a nearly-zero accuracy if a model is not trained by an adversarial attack-aware strategy, *e.g.*, adversarial training [20, 61]. On

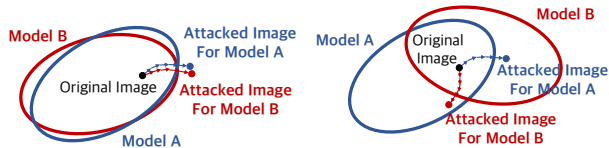


Figure 2: **Relationship between adversarial attack transferability and decision boundary.** If two models have similar decision boundaries, generated adversarial samples for one model can fool another model (**left**). On the other hand, generated adversarial samples for one model cannot fool another model having dissimilar boundaries (**right**).

the other hand, if the adversarial attacks on A are not transferable to B and vice versa, then $s(A, B) = \log \varepsilon_s$.

Eq. (1) can act as a similarity function from the functional point of view. Ideally, we would like to define a similarity function between two models with the following three properties: (1) $x = \arg \min_y d(x, y)$, (2) $d(x, y) = d(y, x)$ and (3) $d(x, y) > d(x, x)$ if $x \neq y$. The proposed function generally satisfies these properties. If we assume the adversary is optimal, then $\text{acc}_{A \rightarrow A}$ will be zero, and it will be the minimum (because accuracy is non-negative). “ $\text{acc}_{A \rightarrow B} + \text{acc}_{B \rightarrow A}$ ” is symmetric. It will satisfy $d(x, y) \geq d(x, x)$ if $x \neq y$ where it is a weaker condition than (3).

Now, we extensively analyze numerous state-of-the-art networks using our quantity, by focusing on two questions. (1) Which network component contributes to the diversity between models? (2) Why do we need to develop various neural architectures? We observe the answers to the two questions with in-depth analysis using 69 recent ImageNet models based on our similarity.

Settings. We use the projected gradient descent (PGD) for the adversary. We set the iteration to 50, the learning rate to 0.1, and ε to $8/255$ for the PGD attack. We select 69 neural architectures trained on ImageNet [72] from the PyTorch Image Models library¹ [99]. Notice that to reduce the unexpected effect of a significant accuracy gap, the chosen model candidates are limited to the models whose top-1 accuracy is between 79% and 83%. We also ignore the models with unusual training techniques, such as training on extra training datasets, using a small or large model input resolution (*e.g.*, less than 200 or larger than 300), or knowledge distillation. When A and B take different input resolutions, then we resize the attacked image from the source network for the target network. We also sub-sample 10% ImageNet validation images (*i.e.*, 5,000 images) to measure the similarity. This strategy makes our similarity score more computationally efficient. The full pairwise similarities of 69 models can be found in Appendix.

¹<https://github.com/rwightman/pytorch-image-models>

Somepalli <i>et al.</i> [78]		Ours	
# triplets	std	# images	std
10	4.49	500	1.88
20	3.28	1000	1.05
50	1.63	2500	0.91
100	1.54	5000	0.77

Table 1: **Comparison of stability of measurements.** We compare the stability of method by [78] and our method. Stability is indicated by the standard deviation (std).

Comparison. Somepalli *et al.* [78] have explored the use of decision boundaries to compare models. However, our method has two advantages over Somepalli *et al.*, namely, computational efficiency and the reliability of the results. First, our approach involves sampling 5,000 images and using 50-step PGD. In this case, the whole amount of the inference becomes $(5,000 \text{ (sampled images)} \times 50 \text{ (PGD steps)} + 5,000 \text{ (test to another model)}) \times 2 \text{ (two models)}$. On the other hand, Somepalli *et al.* [78] sample 500 triplets and generate 2,500 points to construct decision boundaries. In this case, the whole amount of inference is $(500 \text{ (sampled triplets)} \times 2,500 \text{ (grid points)}) \times 2 \text{ (two models)}$, which is about five times greater than our method. Secondly, the approach proposed in [78] samples three images belonging to different classes (*i.e.*, “triplet”). The original paper uses the CIFAR-10 dataset [51], which has only ten classes. Here, 500 triplets can cover all possible combinations of three classes among the ten classes ($\binom{10}{3} = 120 < 500$). However, in datasets with a large number of classes, it becomes computationally infeasible to represent all possible combinations of three classes (*e.g.*, $\binom{1000}{3} = 164,335,500$, almost 130 times greater than the number of training examples of ImageNet). Additionally, we find that the similarity results are reliable (*i.e.*, showing a high variance) when the number of sample triplets is small. In Tab. 1, we calculate the similarity scores between ConvNeXt-T [60] and Swin-T [59] from ten different sets with varying sample sizes. Our method exhibits significantly better stability (*i.e.*, low variances) than Somepalli *et al.* Note that we use our similarity measurement as the percentage degree without the logarithmic function and control the scale of samples to maintain similar computation complexity between ours and the compared method for a fair comparison.

4. Model analysis by network similarity

We quantitatively analyze how each model component affects the similarity or diversity between networks by feature importance analysis and clustering analysis (Sec. 4.1). We also show that the diversity caused by different training strategies is not as significant as caused by different neural architectures (Sec. 4.2).

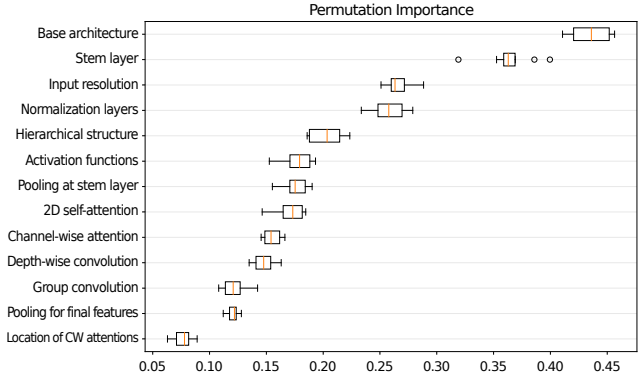


Figure 3: **Importance of architectural components to network similarity.** 13 components (Tab. 2) are sorted by the contribution to the network similarities. The larger feature importance means the component contributes more to the network similarity.

4.1. Which architectural component causes the difference most?

Settings. We list 13 components of each architecture, *e.g.*, normalization (*e.g.*, BN [46] and LN [2]), activation functions (*e.g.*, ReLU [52] and GeLU [71]) the existence of depthwise convolution, or stem layer (*e.g.*, 7×7 conv, 3×3 conv, or 16×16 conv with stride 16 – a.k.a. “patchify” stem [60]). The list of sub-modules is shown in Tab. 2 and Appendix. We then convert each architecture as a feature vector based on the listed sub-modules. For example, we convert ResNet as $f_{\text{ResNet}} = [\text{Base arch} = \text{CNN}, \text{Norm} = \text{BN}, \text{Activation} = \text{ReLU}, \dots]$.

Feature important analysis. The full list of components of 69 architectures is in Appendix. Now, we measure the feature importance by fitting a gradient boosting regressor [28] on the feature difference (*e.g.*, $f_{\text{ResNet-50}} - f_{\text{DeiT-base}}$) measured by Hamming distance and the corresponding similarity. The details of the regressor are described in Appendix. We use the permutation importance [6] that indicates how the trained regression model changes the prediction according to randomly changing each feature. The feature importance of each architectural component is shown in Fig. 3. We first observe that the choice of base architecture (*e.g.*, CNN [52], Transformer [94], and MLP-Mixer [87]) contributes to the similarity most significantly. Fig. 3 also shows that the design choice of the input layer (*i.e.*, stem layer design choice or input resolution) affects the similarity as much as the choice of basic components such as normalization layers, activation functions, and the existence of attention layers. On the other hand, we observe that the modified efficiency-aware convolution operations, such as depth-wise convolution [16] or group convolution [102], are ineffective for model diversity.

Components	Elements
Base architecture	CNN, Transformer, MLP-Mixer, Hybrid (CNN + Transformer), NAS-Net
Stem layer	7×7 conv with stride 2, 3×3 conv with stride 2, 16×16 conv with stride 16, ...
Input resolution	224×224, 256×256, 240×240, 299×299
Normalization layer	BN, GN, LN, LN + GN, LN + BN, Normalization-free, ...
Using hierarchical structure	Yes (<i>e.g.</i> , CNNs, Swin [59]), No (<i>e.g.</i> , ViT [26])
Activation functions	ReLU, HardSwish, SiLU, GeLU, ReLU + GeLU, ReLU + SiLU or GeLU ...
Using pooling at stem	Yes, No
Using 2D self-attention	Yes (<i>e.g.</i> , [4], [80], [93]), No
Using channel-wise (CW) attention	Yes (<i>e.g.</i> , [44], [9], [98]), No
Using depth-wise convolution	Yes, No
Using group convolution	Yes, No
Type of pooling for final feature	Classification (CLS) token, Global Average Pool (GAP)
Location of CW attentions	At the end of each block, in the middle of each block, ...

Table 2: **Overview of model elements.** We categorize each architecture with 13 different architectural components. The full feature list of each architecture is in Appendix.

Clustering analysis. We additionally provide a clustering analysis based on the architectural similarities. We construct a pairwise similarity graph A between all 69 architectures where its vertex denotes an architecture, and its edge denotes the similarity between two networks. We perform the spectral clustering algorithm [64] on A where the number of clusters K is set to 10: We compute the Laplacian matrix of A , $L = D - A$ where D is the diagonal matrix and its i -th component is $\sum_j A_{ij}$. Then, we perform K-means clustering on the K -largest eigenvectors of L , where K is the number of clusters (*i.e.*, $K = 10$). The pairwise distances of spectral features (*i.e.*, 10-largest eigenvectors of L) of 69 neural architectures are shown in Fig. 4a. The rows and columns of Fig. 4a are sorted by the clustering index of Tab. 3. We can see the block-diagonal patterns, *i.e.*, in-clusters similarities are more significant than between-clusters similarities. More details of spectral clustering are introduced in Appendix.

Tab. 3 shows the clustering results on 69 networks and the top-5 keywords for each cluster based on term frequency-inverse document frequency (TF-IDF) analysis. Specifically, we treat each model feature (Tab. 2) as a word and compute TF and IDF by treating each architecture as a document. Then we compute the average TF-IDF for each cluster and report top-5 keywords. Similar to Fig. 3, the base architecture (*e.g.*, CNN in Cluster 5, 6, 10 and Transformer in Cluster 2, 3) and the design choice for the stem layer (*e.g.*, Cluster 1, 2, 4, 5, 6, 7, 8, 10) repeatedly appear at the top keywords. Especially, we can observe that the differences in base architecture significantly cause the diversity in model similarities, *e.g.*, non-hierarchical Transformers (Cluster 1), hierarchical networks with the patchification stem (Cluster 2), hierarchical Transformers (Cluster 3), CNNs with 2D self-attention (Cluster 4, 5), ResNet-based architectures (Cluster 6), and NAS-based architectures (Cluster 7).

4.2. Training strategy and similarity score

The architectural difference is not the only cause of the model diversity. We compare the effect by different architecture choices (*e.g.*, ResNet and ViT) and by different training strategies while fixing the model architecture, as follows: **Different initializations** can affect the model training by the nature of the stochasticity of the training procedure. For example, Sompalli *et al.* [78] showed that the decision boundary of each architecture could vary by different initializations. We also consider **different optimization hyper-parameters** (*e.g.*, learning rate, weight decay). Finally, we study the effect of **different training regimes** (*e.g.*, augmentations, type of supervision). For example, the choice of data augmentation (*e.g.*, Mixup [109], or CutMix [106]) or the optimization techniques (*e.g.*, [84]) can theoretically or empirically affect adversarial robustness [19, 65, 74, 111]. Similarly, we investigate the effect of different types of supervision, such as self-supervision (*e.g.*, MOCO [12], MAE [38] and BYOL [33]) or semi-weakly supervised learning [103]. Experimental details about the used models are provided in Appendix.

Tab. 4 shows the comparison of similarity scores between the same architecture but different learning methods (a smaller similarity means more diversity). First, we observe that using different random initialization or different optimization hyper-parameters shows high correlations with each other (almost ≥ 4.2) while the average similarity score between various neural architectures is 2.73. In other words, the difference in initializations or optimization hyper-parameters does not significantly contribute to the model diversity. Second, we observe that using different learning technique (*e.g.*, different augmentation methods and different types of supervision) remarkably affect the similarity score (3.27 for ResNet and 3.44 for ViT), but is not as significant as the architectural difference (2.73). Furthermore, the change of similarity caused by different

No.	Top-5 Keywords	Architecture
1	Stem layer: 16×16 conv w/ s16, No Hierarchical, GeLU, LN, Final GAP	ConViT-B [27], CrossViT-B [10], DeiT-B [89], DeiT-S [89], ViT-S (patch size 16) [26], ResMLP-S24 [88], gMLP-S [58]
2	Stem layer: 4×4 conv w/ s4, LN, GeLU, Transformer, No pooling at stem	Twins-PCPVT-B [17], Twins-SVT-S [17], CoaT-Lite Small [23], NesT-T [113], Swin-T [59], S3 (Swin-T) [11], ConvNeXt-T [60], ResMLP-B24 [88]
3	Transformer, Final GAP, GeLU, Pooling at stem, InRes: 224	XCiT-M24 [1], XCiT-T12 [1], HaloRegNetZ-B [†] , TNT-S [37], Visformer-S [14], PiT-S [42], PiT-B [42]
4	Stem layer: stack of 3×3 conv, 2D SA, InRes: 256, Pooling at stem, SiLU	HaloNet-50 [93], LambdaResNet-50 [4], BoTNet-26 [80], GC-ResNeXt-50 [9], ECAHaloNeXt-50 [†] , ECA-BoTNeXt-26 [†]
5	Stem layer: stack of 3×3 convs, InRes: 256, 2D SA, CWA: middle of blocks, CNN	LamHaloBoTNet-50 [†] , SE-BoTNet-33 [†] , SE-HaloNet-33 [†] , Halo2BoTNet-50 [†] , GC-ResNet-50 [9], ECA-Net-33 [98]
6	Stem layer: 7×7 conv w/ s2, ReLU, Pooling at stem, CNN, BN	ResNet-50 [39], ResNet-101 [39], ResNeXt-50 [102], Wide ResNet-50 [108], SE-ResNet-50 [44], SE-ResNeXt-50 [44], ResNet-V2-50 [40], ResNet-V2-101 [40], ResNet-50 (GN) [101], ResNet-50 (BlurPool) [112], DPN-107 [13], Xception-65 [16]
7	NAS, Stem layer: 3×3 conv w/ s2 CWA: middle of blocks, CWA, DW Conv	EfficientNet-B2 [85], FBNetV3-G [22], ReXNet (×1.5) [36], RegNetY-32 [69], MixNet-XL [86], NF-RegNet-B1 [7]
8	Input resolution: 224, Stem layer: stack of 3×3 convs, Group Conv, Final GAP, 2D SA	NFNet-L0 [†] , ECA-NFNet-L0 [†] , PoolFormer-M48 [105], ResNeSt-50 [110], ResNet-V2-50-D-EVOS [†] , ConvMixer-1536/20 [91]
9	ReLU, Input resolution: 224, DW Conv, BN, 2D self-attention	ViT-B (patch size 32) [26], R26+ViT-S [81], DLA-X-102 [104], eSE-VoVNet-39 [55], ResNet-101-C [41], RegNetX-320 [69], HRNet-W32 [97]
10	ReLU + Leaky ReLU, InRes: 256, Stem layer: 7×7 conv, CNN, Pooling at stem	CSPResNet-50 [96], CSPResNeXt-50 [96], CSPDarkNet-53 [5], NF-ResNet-50 [7]

Table 3: **Clustering by similarities.** We perform a clustering analysis on 69 architectures. All the architectures here are denoted by the aliases defined in their respective papers. We show the top-5 keywords for each cluster based on TF-IDF. InRes, SA, and CWA denote input resolution, self-attention, and channel-wise attention, respectively. The customized model details are described in the footnote[†].

Architecture	Diversity by	Similarity
ResNet-50	Initialization	4.23
	Hyper-parameter	4.05
	Training regime	3.27
ViT-S	Initialization	4.21
	Hyper-parameter	4.22
	Training regime	3.44
All		2.73

Table 4: **Similarity within the same architecture.** We compare the average similarity within the same network architecture but trained with different procedures, *e.g.*, random initializations, optimization hyper-parameters, and different training regimes. We report the similarities of two neural architectures, ResNet-50 and ViT-S. “All” denotes the average similarity of 69 neural architectures in Tab. 3.

initializations or hyper-parameters is less marked than the change caused by different architecture (Fig. 4b). This indicates constructing new architecture is a more efficient way to achieve varied models rather than re-training the same one. The need for diversity is observed in the next section.

5. Analysis for Ensemble and Distillation

In this section, we observe neural architecture-related phenomena using our similarity function. First, we show that using more diverse models will lead to better ensemble performance (Sec. 5.1). Second, we study the relationship between knowledge distillation and similarity score. Furthermore, we can suggest a similarity-based guideline for

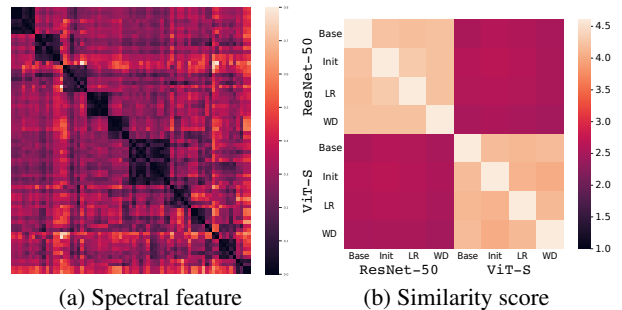


Figure 4: **Spectral feature from similarity and similarity score of ResNet-50 and ViT-s with four different optimization settings.** The rows and columns of (a) are sorted by the clustering index of Tab. 3. More details with model names are described in Appendix. Init, LR, and WD are randomly chosen from models trained with different settings of initialization, learning rate, and weight decay in Tab. 4, respectively.

choosing a teacher model when distilling to a specific architecture. Through these observations, we can provide insights into the necessity of diverse models.

5.1. Model diversity and ensemble performance

The model ensemble is a practical technique to achieve high performances in practice. However, few works study the relationship between ensemble performance and model

[†]Customized models by [99]: HaloRegNetZ = HaloNet + RegNetZ; ECA-BoTNeXt = ECA-Net + HaloNet + ResNeXt; ECA-BoTNeXt = ECA-Net + BoTNet + ResNeXt; LamHaloBoTNet = LambdaNet + HaloNet + BoTNet; SE-BoTNet = SENet + BoTNet; SE-HaloNet = SENet + HaloNet; Halo2BoTNet = HaloNet + BoTNet; NFNet-L0 = an efficient variant of NFNet-F0 [8]; ECA-NFNet-L0 = ECA-Net + NFNet-L0; ResNet-V2-D-EVOS = ResNet-V2 + EvoNorms [57].

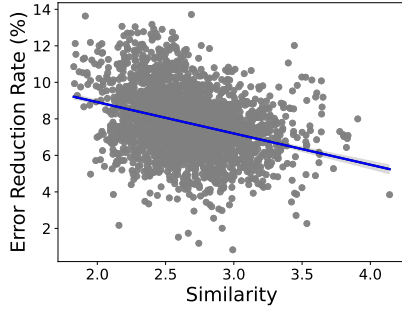
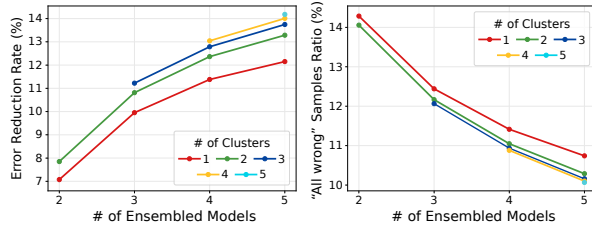


Figure 5: **Correlation between model similarity and ensemble performance.** The trend line and its 90% confidence interval are shown in the blue line.



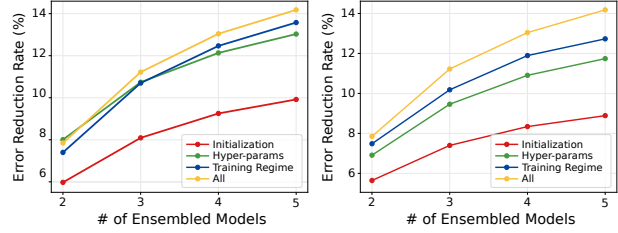
(a) Error reduction rate (b) “All wrong” samples ratio

Figure 6: **Model diversity by architecture difference and ensemble performance.** We report ensemble performances by varying the number of ensembled models (N) and the diversity of the ensembled models. The diversity is controlled by choosing the models from k different clusters (larger k denotes more diversity).

similarity, particularly for large-scale complex models. Previous studies are mainly conducted on tiny datasets and linear models [53]. We investigate the change of ensemble performance according to the change of similarity based on the unweighted average method [48] (*i.e.*, averaging the logit values of the ensembled models). Because the ensemble performance is sensitive to the original model performances, we define Error Reduction Rate (ERR) as $1 - \frac{\text{Err}_{\text{ens}}(M)}{\frac{1}{|M|} \sum_{m \in M} \text{Err}(m)}$, where M is the set of the ensembled models, $\text{Err}(m)$ denotes the top-1 ImageNet validation error of model m , and $\text{Err}_{\text{ens}}(\cdot)$ denotes the top-1 error of the ensemble.

We first measure the 2-ensemble performances among the 69 neural architectures in Tab. 3 (*i.e.*, the number of ensembles is $\binom{69}{2} = 2346$). We plot the relationship between the model similarity and ERR in Fig. 5. We observe that there exists a strong negative correlation between the model similarity and the ensemble performance (Pearson correlation coefficient -0.31 with p-value 1.74×10^{-54}), *i.e.*, *more diversity leads to better ensemble performance.*

We also conduct N -ensemble experiments with $N \geq 2$ based on the clustering results in Tab. 3. We evaluate the average ERR of the ensemble of models from k clusters, *i.e.*, if $N = 5$ and $k = 3$, the ensembled models are only sampled from the selected 3 clusters while ignoring the other 7



(a) ResNet-50 (b) ViT-S

Figure 7: **Model diversity by training techniques and ensemble performance.** The same metrics to Fig. 6 for ResNet-50 and ViT-S models in Tab. 4 are shown. “All” means $N=k$ in Fig. 6 (*i.e.*, # of ensembled models = # of Clusters).

clusters. We investigate the effect of model diversity and ensemble performance by examining $k = 1 \dots N$ (*i.e.*, larger k denotes more diverse ensembled models). We report the result with the metric, error reduction rate (higher is better) in Fig. 6a. ImageNet top-1 error of the ensemble is also shown in Appendix. In all metrics, we observe that the ensemble of more diverse models (*i.e.*, by increasing the number of clusters for the model selection) shows better ensemble performance. Interestingly, in Fig. 6a, we observe that when the number of clusters for the model selection (k) is decreased, the ensemble performance by the number of ensembled models (N) quickly reaches saturation. Similarly, in Fig. 6b, we observe that the number of wrong samples by all models is decreased by selecting more diverse models. In other words, the different architectural choices can lead to different model decision boundaries.

In Sec. 4.2, we showed that the different training strategies are not as effective as different architectures in terms of diversity. To examine the effect of this observation on the ensemble scenario, we report the ensemble results of different training strategies, *i.e.*, the same ResNet-50 and ViT-S models in Tab. 4. For comparison with different architectures, we also report the ensemble of different architectures where all ensembled models are from different clusters (*i.e.*, when $N = k$ in Fig. 6). Fig. 7 shows that although using diverse training regimes (blue lines) improves ensemble performance most among other training techniques (red and green lines), the improvements by using different architectures (yellow lines) are more significant than the improvements by using different training regimes (blue lines) with large gaps.

5.2. Model diversity and knowledge distillation

Knowledge distillation [43] is a training method for transferring rich knowledge of a well-trained teacher network. Intuitively, distillation performance affects a lot by choice of the teacher network; however, the relationship between similarity and distillation performance has not yet been explored enough, especially for ViT. This subsection

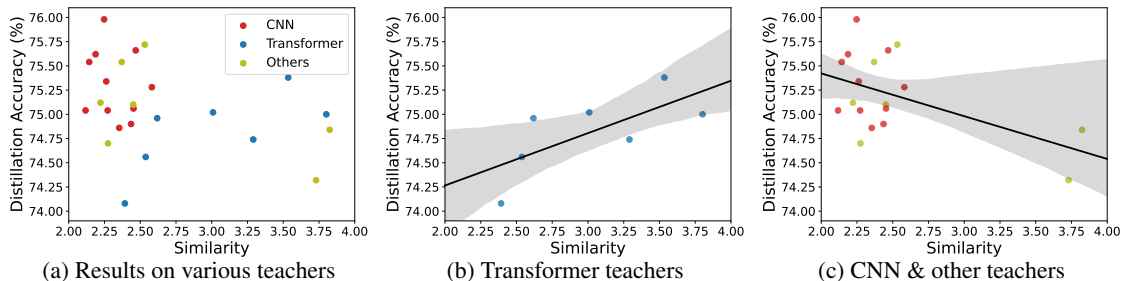


Figure 8: **Model diversity and distillation performance.** (a) We show the relationship between teacher-student similarity and distillation performance of 25 DeiT-S models distilled by various teacher networks. We show the relationship when the teacher and student networks are based on (b) Transformer and (c) otherwise.

investigates how the similarity between teacher and student networks contributes to the distillation performance. There are several studies showing two contradictory conclusions; Jin *et al.* [47] and Mirzadeh *et al.* [63] showed that a similar teacher leads to better distillation performance; Touvron *et al.* [89] reports that distillation from a substantially different teacher is beneficial for ViT training.

We train 25 ViT-Ti models with different teacher networks from Tab. 3 by the hard distillation strategy [43]. Experimental details are described in Appendix. Fig. 8a illustrates the relationship between the teacher-student similarity and the distillation performance. Fig. 8a tends to show a not significant negative correlation between teacher-student similarity and distillation performance (-0.32 Pearson correlation coefficient with 0.12 p-value). However, if we only focus on when the teacher and student networks are based on the same architecture (*i.e.*, Transformer), we can observe a strong positive correlation (Fig. 8b) -0.70 Pearson correlation coefficient with 0.078 p-value. In this case, our observation is aligned with [47, 63]: a teacher similar to the student improves distillation performance. However, when the teacher and student networks are based on different architectures (*e.g.*, CNN), then we can observe a stronger negative correlation (Fig. 8c) with -0.51 Pearson correlation coefficient and 0.030 p-value. In this case, a more dissimilar teacher leads to better distillation performance. We also test other factors that can affect distillation performance in Appendix; We observe that distillation performance is not correlated to teacher accuracy in our experiments.

Why do we observe contradictory results for Transformer teachers (Fig. 8b) and other teachers (Fig. 8c)? Here, we conjecture that when the teacher and student networks differ significantly, distillation works as a strong regularizer. In this case, using a more dissimilar teacher can be considered a stronger regularizer (Fig. 8c). On the other hand, we conjecture that if two networks are similar, then distillation works as easy-to-follow supervision for the student network. In this case, we can assume that a more similar teacher will work better because a more similar teacher will provide more easy-to-follow supervision for the student network (Fig. 8b). Our experiments show that the regular-

ization effect improves distillation performance better than easy-to-follow supervision (*i.e.*, the best-performing distillation result is by a CNN teacher). Therefore, in practice, we recommend using a significantly different teacher network for achieving better distillation performance (*e.g.*, using RegNet [69] teacher for ViT student as [89]).

6. Limitations and discussions

We include three discussions related to our similarity score. Due to the space limit, the full details of each item can be found in Appendix. Our discussions include:

- Robustness of our similarity score to the choice of adversarial attack method. We show that the similarity rankings by PGD [61], AutoAttack [21], and Patch-Fool [29] do not differ significantly.
- How adversarially trained models affect our similarity scores.
- An efficient approximation of our analysis for a novel model (*i.e.*, for a novel 70th model for our analysis). We show that instead of generating adversarial attacks for all 70 models, just using the attacked images from the novel model could be enough.
- Other possible applications of our similarity score (*e.g.*, a novel architecture development, analyzing the hyper-parameter sensitivity, model selection for selecting diverse models).

7. Conclusion

We have explored similarities between image classification models to investigate what makes the model similar or diverse and whether developing and using diverse models are required. For quantitative and model-agnostic assessment of the similarity, we have suggested a new similarity function based on attack transferability demonstrating differences in input gradients and decision boundaries. Using our new similarity function, we conduct a large-scale and extensive analysis using 69 state-of-the-art ImageNet models. We have shown that macroscopic architectural properties, such as base architecture and stem architecture, have a

more significant impact on similarity than microscopic operations, such as types of used convolution, with numerical analysis. Furthermore, the effectiveness of the training strategy is minor compared to model architectural design-related features. Finally, we have firstly discovered the advantages of using diverse models in ensemble or distillation strategies for a practical scenario with a large-scale training dataset and a highly complex architecture.

Author Contributions

This work is done as an internship project by J Hwang under the supervision of S Chun. S Chun initialized the project idea: understanding how different architectures behave differently by using an adversarial attack. J Hwang, S Chun, and D Han jointly designed the analysis toolbox. J Hwang implemented the analysis toolbox and conducted the experiments with input from S Chun, D Han, and J Lee. J Hwang, D Han, B Heo, and S Chun contributed to interpreting and understanding various neural architectures under our toolbox. The initial version of “model card” (Tab. A.2 and A.3) was built by J Hwang, S Park, and verified by D Han and B Heo. B Heo contributed to interpreting distillation results. All ResNet and ViT models newly trained in this work were trained by S Park. J Lee supervised J Hwang and verified the main idea and experiments during the project. S Chun and J Hwang wrote the initial version of the manuscript. All authors contributed to the final manuscript.

Acknowledgement

We thank Taekyung Kim and Namuk Park for providing valuable comments on the self-supervised pre-training.

References

- [1] Alaaeldin Ali, Hugo Touvron, Mathilde Caron, Piotr Bojanowski, Matthijs Douze, Armand Joulin, Ivan Laptev, Natalia Neverova, Gabriel Synnaeve, Jakob Verbeek, et al. Xcit: Cross-covariance image transformers. In *Adv. Neural Inform. Process. Syst.*, 2021. 6
- [2] Jimmy Lei Ba, Jamie Ryan Kiros, and Geoffrey E Hinton. Layer normalization. *arXiv preprint arXiv:1607.06450*, 2016. 1, 4
- [3] Naman Bansal, Chirag Agarwal, and Anh Nguyen. Sam: The sensitivity of attribution methods to hyperparameters. In *IEEE Conf. Comput. Vis. Pattern Recog.*, 2020. 1, 2
- [4] Irwan Bello. Lambdanetworks: Modeling long-range interactions without attention. In *Int. Conf. Learn. Represent.*, 2021. 5, 6
- [5] Alexey Bochkovskiy, Chien-Yao Wang, and Hong-Yuan Mark Liao. Yolov4: Optimal speed and accuracy of object detection. *arXiv preprint arXiv:2004.10934*, 2020. 6
- [6] Leo Breiman. Random forests. *Machine learning*, 45(1):5–32, 2001. 4
- [7] Andrew Brock, Soham De, and Samuel L Smith. Characterizing signal propagation to close the performance gap in unnormalized resnets. In *Int. Conf. Learn. Represent.*, 2021. 6
- [8] Andy Brock, Soham De, Samuel L Smith, and Karen Simonyan. High-performance large-scale image recognition without normalization. In *Int. Conf. Mach. Learn.*, 2021. 6
- [9] Yue Cao, Jiarui Xu, Stephen Lin, Fangyun Wei, and Han Hu. Gcnet: Non-local networks meet squeeze-excitation networks and beyond. In *Int. Conf. Comput. Vis. Worksh.*, 2019. 5, 6
- [10] Chun-Fu Richard Chen, Quanfu Fan, and Rameswar Panda. Crossvit: Cross-attention multi-scale vision transformer for image classification. In *Int. Conf. Comput. Vis.*, 2021. 6
- [11] Minghao Chen, Kan Wu, Bolin Ni, Houwen Peng, Bei Liu, Jianlong Fu, Hongyang Chao, and Haibin Ling. Searching the search space of vision transformer. In *Adv. Neural Inform. Process. Syst.*, 2021. 6
- [12] Xinlei Chen, Saining Xie, and Kaiming He. An empirical study of training self-supervised vision transformers. *Int. Conf. Comput. Vis.*, 2021. 5, 18
- [13] Yunpeng Chen, Jianan Li, Huaxin Xiao, Xiaojie Jin, Shuicheng Yan, and Jiashi Feng. Dual path networks. In *Adv. Neural Inform. Process. Syst.*, 2017. 6
- [14] Zhengsu Chen, Lingxi Xie, Jianwei Niu, Xuefeng Liu, Longhui Wei, and Qi Tian. Visformer: The vision-friendly transformer. In *Int. Conf. Comput. Vis.*, 2021. 6
- [15] Junsuk Choe, Seong Joon Oh, Sanghyuk Chun, and Hyunjung Akata, Zeynepand Shim. Evaluation for weakly supervised object localization: Protocol, metrics, and datasets. *IEEE Trans. Pattern Anal. Mach. Intell.*, 2022. 1, 2, 21
- [16] François Chollet. Xception: Deep learning with depthwise separable convolutions. In *IEEE Conf. Comput. Vis. Pattern Recog.*, 2017. 4, 6
- [17] Xiangxiang Chu, Zhi Tian, Yuqing Wang, Bo Zhang, Haibing Ren, Xiaolin Wei, Huaxia Xia, and Chunhua Shen. Twins: Revisiting the design of spatial attention in vision transformers. In *Adv. Neural Inform. Process. Syst.*, 2021. 6
- [18] Sanghyuk Chun, Wonjae Kim, Song Park, Minsuk Chang Chang, and Seong Joon Oh. Eccc caption: Correcting false negatives by collecting machine-and-human-verified image-caption associations for ms-coco. In *Eur. Conf. Comput. Vis.*, 2022. 21
- [19] Sanghyuk Chun, Seong Joon Oh, Sangdoon Yun, Dongyoon Han, Junsuk Choe, and Youngjoon Yoo. An empirical evaluation on robustness and uncertainty of regularization methods. In *Int. Conf. Mach. Learn. Worksh.*, 2019. 5
- [20] Jeremy Cohen, Elan Rosenfeld, and Zico Kolter. Certified adversarial robustness via randomized smoothing. In *Int. Conf. Mach. Learn.*, 2019. 3
- [21] Francesco Croce and Matthias Hein. Reliable evaluation of adversarial robustness with an ensemble of diverse parameter-free attacks. In *Int. Conf. Mach. Learn.*, 2020. 1, 3, 8, 19
- [22] Xiaoliang Dai, Alvin Wan, Peizhao Zhang, Bichen Wu, Zijian He, Zhen Wei, Kan Chen, Yuandong Tian, Matthew Yu, Peter Vajda, et al. Fbnetv3: Joint architecture-recipe search using predictor pretraining. In *IEEE Conf. Comput. Vis.*

- Pattern Recog.*, 2021. 6
- [23] Zihang Dai, Hanxiao Liu, Quoc V Le, and Mingxing Tan. Coatnet: Marrying convolution and attention for all data sizes. In *Adv. Neural Inform. Process. Syst.*, 2021. 6
- [24] Terrance DeVries and Graham W Taylor. Improved regularization of convolutional neural networks with cutout. *arXiv preprint arXiv:1708.04552*, 2017. 18
- [25] Laurent Dinh, Razvan Pascanu, Samy Bengio, and Yoshua Bengio. Sharp minima can generalize for deep nets. In *Int. Conf. Mach. Learn.*, 2017. 1, 2
- [26] Alexey Dosovitskiy, Lucas Beyer, Alexander Kolesnikov, Dirk Weissenborn, Xiaohua Zhai, Thomas Unterthiner, Mostafa Dehghani, Matthias Minderer, Georg Heigold, Sylvain Gelly, Jakob Uszkoreit, and Neil Houlsby. An image is worth 16x16 words: Transformers for image recognition at scale. In *Int. Conf. Learn. Represent.*, 2021. 5, 6, 18
- [27] Stéphane d’Ascoli, Hugo Touvron, Matthew L Leavitt, Ari S Morcos, Giulio Biroli, and Levent Sagun. Convit: Improving vision transformers with soft convolutional inductive biases. In *Int. Conf. Mach. Learn.*, 2021. 6
- [28] Jerome H Friedman. Greedy function approximation: a gradient boosting machine. *Annals of statistics*, pages 1189–1232, 2001. 4, 13
- [29] Yonggan F Fu, Shang Wu, Yingyan Lin, et al. Patch-fool: Are vision transformers always robust against adversarial perturbations? *Int. Conf. Learn. Represent.*, 2022. 8, 19
- [30] Robert Geirhos, Kristof Meding, and Felix A Wichmann. Beyond accuracy: quantifying trial-by-trial behaviour of cnns and humans by measuring error consistency. In *Adv. Neural Inform. Process. Syst.*, 2020. 2
- [31] Robert Geirhos, Carlos RM Temme, Jonas Rauber, Heiko H Schütt, Matthias Bethge, and Felix A Wichmann. Generalisation in humans and deep neural networks. In *Adv. Neural Inform. Process. Syst.*, 2018. 2
- [32] Ian J Goodfellow, Jonathon Shlens, and Christian Szegedy. Explaining and harnessing adversarial examples. In *Int. Conf. Learn. Represent.*, 2015. 1
- [33] Jean-Bastien Grill, Florian Strub, Florent Althé, Corentin Tallec, Pierre Richemond, Elena Buchatskaya, Carl Doersch, Bernardo Avila Pires, Zhaohan Guo, Mohammad Gheshlaghi Azar, et al. Bootstrap your own latent—a new approach to self-supervised learning. In *Adv. Neural Inform. Process. Syst.*, 2020. 5, 18
- [34] Ishaan Gulrajani and David Lopez-Paz. In search of lost domain generalization. In *Int. Conf. Learn. Represent.*, 2021. 21
- [35] Jian Guo, He He, Tong He, Leonard Lausen, Mu Li, Haibin Lin, Xingjian Shi, Chenguang Wang, Junyuan Xie, Sheng Zha, Aston Zhang, Hang Zhang, Zhi Zhang, Zhongyue Zhang, Shuai Zheng, and Yi Zhu. Gluoncv and gluonnlp: Deep learning in computer vision and natural language processing. *Journal of Machine Learning Research*, 21(23):1–7, 2020. 18, 20
- [36] Dongyoon Han, Sangdoon Yun, Byeongho Heo, and Youngjoon Yoo. Rethinking channel dimensions for efficient model design. In *IEEE Conf. Comput. Vis. Pattern Recog.*, 2021. 6
- [37] Kai Han, An Xiao, Enhua Wu, Jianyuan Guo, Chunjing Xu, and Yunhe Wang. Transformer in transformer. In *Adv. Neural Inform. Process. Syst.*, 2021. 6
- [38] Kaiming He, Xinlei Chen, Saining Xie, Yanghao Li, Piotr Dollár, and Ross Girshick. Masked autoencoders are scalable vision learners. In *IEEE Conf. Comput. Vis. Pattern Recog.*, 2022. 5, 18
- [39] Kaiming He, Xiangyu Zhang, Shaoqing Ren, and Jian Sun. Deep residual learning for image recognition. In *IEEE Conf. Comput. Vis. Pattern Recog.*, 2016. 1, 6
- [40] Kaiming He, Xiangyu Zhang, Shaoqing Ren, and Jian Sun. Identity mappings in deep residual networks. In *Eur. Conf. Comput. Vis.*, 2016. 6
- [41] Tong He, Zhi Zhang, Hang Zhang, Zhongyue Zhang, Junyuan Xie, and Mu Li. Bag of tricks for image classification with convolutional neural networks. In *IEEE Conf. Comput. Vis. Pattern Recog.*, 2019. 6
- [42] Byeongho Heo, Sangdoon Yun, Dongyoon Han, Sanghyuk Chun, Junsuk Choe, and Seong Joon Oh. Rethinking spatial dimensions of vision transformers. In *Int. Conf. Comput. Vis.*, 2021. 6
- [43] Geoffrey Hinton, Oriol Vinyals, Jeff Dean, et al. Distilling the knowledge in a neural network. In *Adv. Neural Inform. Process. Syst. Worksh.*, 2015. 2, 7, 8
- [44] Jie Hu, Li Shen, and Gang Sun. Squeeze-and-excitation networks. In *IEEE Conf. Comput. Vis. Pattern Recog.*, 2018. 5, 6
- [45] Andrew Ilyas, Shibani Santurkar, Dimitris Tsipras, Logan Engstrom, Brandon Tran, and Aleksander Madry. Adversarial examples are not bugs, they are features. In *Adv. Neural Inform. Process. Syst.*, 2019. 19
- [46] Sergey Ioffe and Christian Szegedy. Batch normalization: Accelerating deep network training by reducing internal covariate shift. In *Int. Conf. Mach. Learn.*, 2015. 1, 4
- [47] Xiao Jin, Baoyun Peng, Yichao Wu, Yu Liu, Jiaheng Liu, Ding Liang, Junjie Yan, and Xiaolin Hu. Knowledge distillation via route constrained optimization. In *Int. Conf. Comput. Vis.*, 2019. 8
- [48] Cheng Ju, Aurélien Bibaut, and Mark van der Laan. The relative performance of ensemble methods with deep convolutional neural networks for image classification. *Journal of Applied Statistics*, 45(15):2800–2818, 2018. 7
- [49] Hamid Karimi and Jiliang Tang. Decision boundary of deep neural networks: Challenges and opportunities. In *Proceedings of the 13th International Conference on Web Search and Data Mining*, 2020. 3
- [50] Simon Kornblith, Mohammad Norouzi, Honglak Lee, and Geoffrey Hinton. Similarity of neural network representations revisited. In *Int. Conf. Mach. Learn.*, 2019. 1, 2
- [51] Alex Krizhevsky, Geoffrey Hinton, et al. Learning multiple layers of features from tiny images. 2009. 4
- [52] Alex Krizhevsky, Ilya Sutskever, and Geoffrey E Hinton. Imagenet classification with deep convolutional neural networks. In *Adv. Neural Inform. Process. Syst.*, 2012. 1, 4
- [53] Ludmila I Kuncheva and Christopher J Whitaker. Measures of diversity in classifier ensembles and their relationship with the ensemble accuracy. *Machine learning*, 51(2):181–207, 2003. 2, 7
- [54] Alina Kuznetsova, Hassan Rom, Neil Alldrin, Jasper Uijlings, Ivan Krasin, Jordi Pont-Tuset, Shahab Kamali, Stefan Popov, Matteo Mallocci, Alexander Kolesnikov, et al.

- The open images dataset v4. *Int. J. Comput. Vis.*, 128(7):1956–1981, 2020. [21](#)
- [55] Youngwan Lee and Jongyoul Park. Centermask: Real-time anchor-free instance segmentation. In *IEEE Conf. Comput. Vis. Pattern Recog.*, 2020. [6](#)
- [56] Hao Li, Zheng Xu, Gavin Taylor, Christoph Studer, and Tom Goldstein. Visualizing the loss landscape of neural nets. In *Adv. Neural Inform. Process. Syst.*, 2018. [2](#)
- [57] Hanxiao Liu, Andy Brock, Karen Simonyan, and Quoc Le. Evolving normalization-activation layers. In *Adv. Neural Inform. Process. Syst.*, 2020. [6](#)
- [58] Hanxiao Liu, Zihang Dai, David So, and Quoc V Le. Pay attention to mlps. In *Adv. Neural Inform. Process. Syst.*, 2021. [6](#)
- [59] Ze Liu, Yutong Lin, Yue Cao, Han Hu, Yixuan Wei, Zheng Zhang, Stephen Lin, and Baining Guo. Swin transformer: Hierarchical vision transformer using shifted windows. In *Int. Conf. Comput. Vis.*, 2021. [4](#), [5](#), [6](#)
- [60] Zhuang Liu, Hanzi Mao, Chao-Yuan Wu, Christoph Feichtenhofer, Trevor Darrell, and Saining Xie. A convnet for the 2020s. In *IEEE Conf. Comput. Vis. Pattern Recog.*, 2022. [4](#), [6](#)
- [61] Aleksander Madry, Aleksandar Makelov, Ludwig Schmidt, Dimitris Tsipras, and Adrian Vladu. Towards deep learning models resistant to adversarial attacks. In *Int. Conf. Learn. Represent.*, 2018. [1](#), [3](#), [8](#), [19](#)
- [62] Kristof Meding, Luca M Schulze Buschoff, Robert Geirhos, and Felix A Wichmann. Trivial or impossible—dichotomous data difficulty masks model differences (on imagenet and beyond). In *Int. Conf. Learn. Represent.*, 2022. [1](#), [2](#)
- [63] Seyed Iman Mirzadeh, Mehrdad Farajtabar, Ang Li, Nir Levine, Akihiro Matsukawa, and Hassan Ghasemzadeh. Improved knowledge distillation via teacher assistant. In *Proceedings of the AAAI Conference on Artificial Intelligence*, 2020. [8](#)
- [64] Andrew Ng, Michael Jordan, and Yair Weiss. On spectral clustering: Analysis and an algorithm. *Adv. Neural Inform. Process. Syst.*, 2001. [5](#)
- [65] Chanwoo Park, Sangdoon Yun, and Sanghyuk Chun. A unified analysis of mixed sample data augmentation: A loss function perspective. In *Adv. Neural Inform. Process. Syst.*, 2022. [5](#)
- [66] Namuk Park and Songkuk Kim. How do vision transformers work? In *Int. Conf. Learn. Represent.*, 2022. [2](#)
- [67] Adam Paszke, Sam Gross, Francisco Massa, Adam Lerer, James Bradbury, Gregory Chanan, Trevor Killeen, Zeming Lin, Natalia Gimelshein, Luca Antiga, et al. Pytorch: An imperative style, high-performance deep learning library. In *Adv. Neural Inform. Process. Syst.*, 2019. [18](#)
- [68] Fabian Pedregosa, Gaël Varoquaux, Alexandre Gramfort, Vincent Michel, Bertrand Thirion, Olivier Grisel, Mathieu Blondel, Peter Prettenhofer, Ron Weiss, Vincent Dubourg, et al. Scikit-learn: Machine learning in python. *Journal of Machine Learning Research*, 12:2825–2830, 2011. [13](#)
- [69] Ilija Radosavovic, Raj Prateek Kosaraju, Ross Girshick, Kaiming He, and Piotr Dollar. Designing network design spaces. In *IEEE Conf. Comput. Vis. Pattern Recog.*, 2020. [6](#), [8](#)
- [70] Maithra Raghu, Thomas Unterthiner, Simon Kornblith, Chiyuan Zhang, and Alexey Dosovitskiy. Do vision transformers see like convolutional neural networks? In *Adv. Neural Inform. Process. Syst.*, 2021. [1](#), [2](#)
- [71] Prajit Ramachandran, Barret Zoph, and Quoc V Le. Searching for activation functions. *arXiv preprint arXiv:1710.05941*, 2017. [4](#)
- [72] Olga Russakovsky, Jia Deng, Hao Su, Jonathan Krause, Sanjeev Satheesh, Sean Ma, Zhiheng Huang, Andrej Karpathy, Aditya Khosla, Michael Bernstein, et al. Imagenet large scale visual recognition challenge. *Int. J. Comput. Vis.*, 2015. [1](#), [2](#), [3](#)
- [73] Luca Scimeca, Seong Joon Oh, Sanghyuk Chun, Michael Poli, and Sangdoon Yun. Which shortcut cues will dnns choose? a study from the parameter-space perspective. In *Int. Conf. Learn. Represent.*, 2022. [2](#)
- [74] Ali Shafahi, Amin Ghiasi, Furong Huang, and Tom Goldstein. Label smoothing and logit squeezing: a replacement for adversarial training? *arXiv preprint arXiv:1910.11585*, 2019. [5](#)
- [75] Karen Simonyan, Andrea Vedaldi, and Andrew Zisserman. Deep inside convolutional networks: Visualising image classification models and saliency maps. In *Int. Conf. Learn. Represent. Worksh.*, 2014. [1](#), [2](#)
- [76] Karen Simonyan and Andrew Zisserman. Very deep convolutional networks for large-scale image recognition. In *Int. Conf. Learn. Represent.*, 2015. [1](#)
- [77] D. Smilkov, N. Thorat, B. Kim, F. Viégas, and M. Wattenberg. Smoothgrad: removing noise by adding noise. *Int. Conf. Mach. Learn. Worksh.*, 2017. [1](#), [2](#)
- [78] Gowthami Somepalli, Liam Fowl, Arpit Bansal, Ping Yeh-Chiang, Yehuda Dar, Richard Baraniuk, Micah Goldblum, and Tom Goldstein. Can neural nets learn the same model twice? investigating reproducibility and double descent from the decision boundary perspective. In *IEEE Conf. Comput. Vis. Pattern Recog.*, 2022. [1](#), [2](#), [4](#), [5](#)
- [79] Jost Tobias Springenberg, Alexey Dosovitskiy, Thomas Brox, and Martin Riedmiller. Striving for simplicity: The all convolutional net. In *Int. Conf. Learn. Represent. Worksh.*, 2015. [1](#), [2](#)
- [80] Aravind Srinivas, Tsung-Yi Lin, Niki Parmar, Jonathon Shlens, Pieter Abbeel, and Ashish Vaswani. Bottleneck transformers for visual recognition. In *IEEE Conf. Comput. Vis. Pattern Recog.*, 2021. [5](#), [6](#)
- [81] Andreas Peter Steiner, Alexander Kolesnikov, Xiaohua Zhai, Ross Wightman, Jakob Uszkoreit, and Lucas Beyer. How to train your vit? data, augmentation, and regularization in vision transformers. In *Transactions on Machine Learning Research*, 2022. [6](#)
- [82] Mukund Sundararajan, Ankur Taly, and Qiqi Yan. Ax- iomatic attribution for deep networks. In *Int. Conf. Mach. Learn.*, 2017. [1](#), [2](#)
- [83] AH Sung. Ranking importance of input parameters of neural networks. *Expert Systems with Applications*, 15(3-4):405–411, 1998. [1](#), [2](#)
- [84] Christian Szegedy, Vincent Vanhoucke, Sergey Ioffe, Jon Shlens, and Zbigniew Wojna. Rethinking the inception architecture for computer vision. In *IEEE Conf. Comput. Vis. Pattern Recog.*, 2016. [5](#)

- [85] Mingxing Tan and Quoc Le. Efficientnet: Rethinking model scaling for convolutional neural networks. In *Int. Conf. Mach. Learn.*, 2019. 6
- [86] Mingxing Tan and Quoc V Le. Mixconv: Mixed depthwise convolutional kernels. In *Brit. Mach. Vis. Conf.*, 2019. 6
- [87] Ilya O Tolstikhin, Neil Houlsby, Alexander Kolesnikov, Lucas Beyer, Xiaohua Zhai, Thomas Unterthiner, Jessica Yung, Andreas Steiner, Daniel Keysers, Jakob Uszkoreit, et al. Mlp-mixer: An all-mlp architecture for vision. In *Adv. Neural Inform. Process. Syst.*, 2021. 4
- [88] Hugo Touvron, Piotr Bojanowski, Mathilde Caron, Matthieu Cord, Alaeldin El-Nouby, Edouard Grave, Gautier Izacard, Armand Joulin, Gabriel Synnaeve, Jakob Verbeek, et al. Resmlp: Feedforward networks for image classification with data-efficient training. *IEEE Trans. Pattern Anal. Mach. Intell.*, 2022. 6
- [89] Hugo Touvron, Matthieu Cord, Matthijs Douze, Francisco Massa, Alexandre Sablayrolles, and Hervé Jégou. Training data-efficient image transformers & distillation through attention. In *Int. Conf. Mach. Learn.*, 2021. 6, 8, 18, 20
- [90] Hugo Touvron, Matthieu Cord, and Hervé Jégou. Deit iii: Revenge of the vit. *arXiv preprint arXiv:2204.07118*, 2022. 18
- [91] Asher Trockman and J. Zico Kolter. Patches are all you need? *arXiv preprint arXiv:2201.09792*, 2022. 6
- [92] Dimitris Tsipras, Shibani Santurkar, Logan Engstrom, Alexander Turner, and Aleksander Madry. Robustness may be at odds with accuracy. In *Int. Conf. Learn. Represent.*, 2019. 18, 19
- [93] Ashish Vaswani, Prajit Ramachandran, Aravind Srinivas, Niki Parmar, Blake Hechtman, and Jonathon Shlens. Scaling local self-attention for parameter efficient visual backbones. In *IEEE Conf. Comput. Vis. Pattern Recog.*, 2021. 5, 6
- [94] Ashish Vaswani, Noam Shazeer, Niki Parmar, Jakob Uszkoreit, Llion Jones, Aidan N Gomez, Lukasz Kaiser, and Illia Polosukhin. Attention is all you need. In *Adv. Neural Inform. Process. Syst.*, 2017. 1, 4
- [95] Vikas Verma, Alex Lamb, Christopher Beckham, Amir Najafi, Ioannis Mitliagkas, David Lopez-Paz, and Yoshua Bengio. Manifold mixup: Better representations by interpolating hidden states. In *Int. Conf. Mach. Learn.*, 2019. 18
- [96] Chien-Yao Wang, Hong-Yuan Mark Liao, Yueh-Hua Wu, Ping-Yang Chen, Jun-Wei Hsieh, and I-Hau Yeh. Cspnet: A new backbone that can enhance learning capability of cnn. In *IEEE Conf. Comput. Vis. Pattern Recog. Worksh.*, 2020. 6
- [97] Jingdong Wang, Ke Sun, Tianheng Cheng, Borui Jiang, Chaorui Deng, Yang Zhao, Dong Liu, Yadong Mu, Mingkui Tan, Xinggang Wang, et al. Deep high-resolution representation learning for visual recognition. *IEEE Trans. Pattern Anal. Mach. Intell.*, 43(10):3349–3364, 2020. 6
- [98] Qilong Wang, Banggu Wu, Pengfei Zhu, Peihua Li, Wangmeng Zuo, and Qinghua Hu. Eca-net: Efficient channel attention for deep convolutional neural networks. In *IEEE Conf. Comput. Vis. Pattern Recog.*, 2020. 5, 6
- [99] Ross Wightman. Pytorch image models. <https://github.com/rwightman/pytorch-image-models>, 2019. 1, 3, 6, 13
- [100] Ross Wightman, Hugo Touvron, and Hervé Jégou. Resnet strikes back: An improved training procedure in timm. In *Adv. Neural Inform. Process. Syst. Worksh.*, 2021. 18
- [101] Yuxin Wu and Kaiming He. Group normalization. In *Eur. Conf. Comput. Vis.*, 2018. 1, 6
- [102] Saining Xie, Ross Girshick, Piotr Dollár, Zhuowen Tu, and Kaiming He. Aggregated residual transformations for deep neural networks. In *IEEE Conf. Comput. Vis. Pattern Recog.*, 2017. 4, 6, 20
- [103] I Zeki Yalniz, Hervé Jégou, Kan Chen, Manohar Paluri, and Dhruv Mahajan. Billion-scale semi-supervised learning for image classification. *arXiv preprint arXiv:1905.00546*, 2019. 5, 18
- [104] Fisher Yu, Dequan Wang, Evan Shelhamer, and Trevor Darrell. Deep layer aggregation. In *IEEE Conf. Comput. Vis. Pattern Recog.*, 2018. 6
- [105] Weihao Yu, Mi Luo, Pan Zhou, Chenyang Si, Yichen Zhou, Xinchao Wang, Jiashi Feng, and Shuicheng Yan. Metaformer is actually what you need for vision. In *IEEE Conf. Comput. Vis. Pattern Recog.*, 2022. 6
- [106] Sangdoon Yun, Dongyoon Han, Seong Joon Oh, Sanghyuk Chun, Junsuk Choe, and Youngjoon Yoo. Cutmix: Regularization strategy to train strong classifiers with localizable features. In *Int. Conf. Comput. Vis.*, 2019. 5, 18
- [107] Sangdoon Yun, Seong Joon Oh, Byeongho Heo, Dongyoon Han, Junsuk Choe, and Sanghyuk Chun. Re-labeling imagenet: from single to multi-labels, from global to localized labels. In *IEEE Conf. Comput. Vis. Pattern Recog.*, 2021. 19
- [108] Sergey Zagoruyko and Nikos Komodakis. Wide residual networks. In *Brit. Mach. Vis. Conf.*, 2016. 6
- [109] Hongyi Zhang, Moustapha Cisse, Yann N Dauphin, and David Lopez-Paz. mixup: Beyond empirical risk minimization. In *Int. Conf. Learn. Represent.*, 2018. 5, 18
- [110] Hang Zhang, Congruo Wu, Zhongyue Zhang, Yi Zhu, Haibin Lin, Zhi Zhang, Yue Sun, Tong He, Jonas Mueller, R. Manmatha, Mu Li, and Alexander Smola. Resnest: Split-attention networks. In *IEEE Conf. Comput. Vis. Pattern Recog. Worksh.*, 2022. 6
- [111] Linjun Zhang, Zhun Deng, Kenji Kawaguchi, Amirata Ghorbani, and James Zou. How does mixup help with robustness and generalization? In *Int. Conf. Learn. Represent.*, 2021. 5
- [112] Richard Zhang. Making convolutional networks shift-invariant again. In *Int. Conf. Mach. Learn.*, 2019. 6
- [113] Zizhao Zhang, Han Zhang, Long Zhao, Ting Chen, Sercan Ö Arik, and Tomas Pfister. Nested hierarchical transformer: Towards accurate, data-efficient and interpretable visual understanding. In *Proceedings of the AAAI Conference on Artificial Intelligence*, 2022. 6

Appendix

We include additional materials in this document, such as the network details (A), spectral clustering method (B), training settings (D), and setting of knowledge distillation (F.1). We also provide experimental results of computing pairwise similarities (C), ensemble performance (E, and distillation performance (F.2). We discuss some limitations and discussion points of our work (G), such as the effect of the choice of attack methods, an efficient approximation, and possible applications.

A. Details of networks used for our analysis

We use 69 models in our research to evaluate the similarity between models and to investigate the impact of model diversity. In the main paper, we mark the names of models based on their research paper and PyTorch Image Models library (`timm`; 0.6.7 version) [99]. Tab. A.1 shows the full list of the models based on their research paper and `timm` alias.

In Tab. A.2 and Tab. A.3, We show the full network specification defined by Tab. 2 of the main paper. We follow the corresponding paper and `timm` library to list the model features.

We fit a gradient boosting regressor [28] based on `Scikit-learn` [68] and report the permutation importance of each component in Fig. 3 of the main paper. The number of boosting stages, maximum depth, minimum number of samples, and learning rate are set to 500, 12, 4, and 0.02, respectively. Permutation importance is computed by permuting a feature 10 times.

Table A.1: Lists of 69 models and their names based on their research paper and `timm` library.

in <code>timm</code>	in paper	in <code>timm</code>	in paper	in <code>timm</code>	in paper
<code>botnet26t_256</code>	BoTNet-26	<code>gluon_xception65</code>	Xception-65	<code>resnet50_gn</code>	ResNet-50 (GN)
<code>coat_lite_small</code>	CoaT-Lite Small	<code>gmlp_s16_224</code>	gMLP-S	<code>resnetblur50</code>	ResNet-50 (BlurPool)
<code>convit_base</code>	ConViT-B	<code>halo2botnet50ts_256</code>	Halo2BoTNet-50	<code>resnetv2_101</code>	ResNet-V2-101
<code>convmixer_1536_20</code>	ConvMixer-1536/20	<code>halonet50ts</code>	HaloNet-50	<code>resnetv2_50</code>	ResNet-V2-50
<code>convnext_tiny</code>	ConvNeXt-T	<code>haloregnetz_b</code>	HaloRegNetZ	<code>resnetv2_50d_evos</code>	ResNet-V2-50-EVOS
<code>crossvit_base_240</code>	CrossViT-B	<code>hrnet_w64</code>	HRNet-W32	<code>resnext50_32x4d</code>	ResNeXt-50
<code>cspdarknet53</code>	CSPDarkNet-53	<code>jx_nest_tiny</code>	NesT-T	<code>rexnet_150</code>	ReXNet (×1.5)
<code>csresnet50</code>	CSPResNet-50	<code>lambda_resnet50ts</code>	LambdaResNet-50	<code>sebotnet33ts_256</code>	SEBoTNet-33
<code>csresnext50</code>	CSPResNeXt-50	<code>lamhalobotnet50ts_256</code>	LamHaloBoTNet-50	<code>sehalonet33ts</code>	SEHaloNet-33
<code>deit_base_patch16_224</code>	DeiT-B	<code>mixnet_xl</code>	MixNet-XL	<code>seresnet50</code>	SEResNet-50
<code>deit_small_patch16_224</code>	DeiT-S	<code>nf_regnet_b1</code>	NF-RegNet-B1	<code>seresnext50_32x4d</code>	SEResNeXt-50
<code>dla102x2</code>	DLA-X-102	<code>nf_resnet50</code>	NF-ResNet-50	<code>swin_s3_tiny_224</code>	S3 (Swin-T)
<code>dpn107</code>	DPN-107	<code>nfnet_l0</code>	NFNet-L0	<code>swin_tiny_patch4_window7_224</code>	Swin-T
<code>eca_botnext26ts_256</code>	ECA-BoTNeXt-26	<code>pit_b_224</code>	PiT-B	<code>tnt_s_patch16_224</code>	TNT-S
<code>eca_halonext26ts</code>	ECA-HaloNeXt-26	<code>pit_s_224</code>	PiT-S	<code>twins_pcpvt_base</code>	Twins-PCPVT-B
<code>eca_nfnet_l0</code>	ECA-NFNet-L0	<code>poolformer_m48</code>	PoolFormer-M48	<code>twins_svt_small</code>	Twins-SVT-S
<code>eca_resnet33ts</code>	ECA-ResNet-33	<code>regnetx_320</code>	RegNetX-320	<code>visformer_small</code>	VisFormer-S
<code>efficientnet_b2</code>	EfficientNet-B2	<code>regnety_032</code>	RegNetY-32	<code>vit_base_patch32_224</code>	ViT-B
<code>ese_vovnet39b</code>	eSE-VoVNet-39	<code>resmlp_24_224</code>	ResMLP-S24	<code>vit_small_patch16_224</code>	ViT-S
<code>fbnetv3_g</code>	FBNetV3-G	<code>resmlp_big_24_224</code>	ResMLP-B24	<code>vit_small_r26_s32_224</code>	R26+ViT-S
<code>gcrenet50t</code>	GCResNet-50	<code>resnest50d</code>	ResNeSt-50	<code>wide_resnet50_2</code>	Wide ResNet-50
<code>gcrenext50ts</code>	GCResNeXt-50	<code>resnet101</code>	ResNet-101	<code>xcit_medium_24_p16_224</code>	XCiT-M24
<code>gluon_resnet101_v1c</code>	ResNet-101-C	<code>resnet50</code>	ResNet-50	<code>xcit_tiny_12_p8_224</code>	XCiT-T12

Table A.2: Description of features of 69 models. “s” in “Stem layer” indicates the stride of a layer in the stem, and the number before and after “s” are a kernel size and size of stride, respectively. For example, “3s2/3/3” means that the stem is composed of the first layer having 3×3 kernel with stride 2, the second layer having 3×3 kernel with stride 1, and the last layer having 3×3 with stride 1.

Model name	Base architecture	Hierarchical structure	Stem layer	Input resolution	Normalization	Activation
botnet26t_256	CNN	Yes	3s2/3/3	256 × 256	BN	ReLU
convmixer_1536_20	CNN	Yes	7s7	224 × 224	BN	GeLU
convnext_tiny	CNN	Yes	4s4	224 × 224	LN	GeLU
cspdarknet53	CNN	Yes	3s1	256 × 256	BN	Leaky ReLU
cspresnet50	CNN	Yes	7s2	256 × 256	BN	Leaky ReLU
cspresnext50	CNN	Yes	7s2	256 × 256	BN	Leaky ReLU
dla102x2	CNN	Yes	7s1	224 × 224	BN	ReLU
dpn107	CNN	Yes	7s2	224 × 224	BN	ReLU
eca_botnext26ts_256	CNN	Yes	3s2/3/3	256 × 256	BN	SiLU
eca_halonext26ts	CNN	Yes	3s2/3/3	256 × 256	BN	SiLU
eca_nfnet_l0	CNN	Yes	3s2/3/3s2	224 × 224	Norm-free	SiLU
eca_resnet33ts	CNN	Yes	3s2/3/3s2	256 × 256	BN	SiLU
ese_vovnet39b	CNN	Yes	3s2/3/3s2	224 × 224	BN	ReLU
gcrsnet50t	CNN	Yes	3s2/3/3s2	256 × 256	LN + BN	ReLU
gcrsnext50ts	CNN	Yes	3s2/3/3	256 × 256	LN + BN	ReLU + SiLU
gluon_resnet101_v1c	CNN	Yes	3s2/3/3	224 × 224	BN	ReLU
gluon_xception65	CNN	Yes	3s2/3	299 × 299	BN	ReLU
halo2botnet50ts_256	CNN	Yes	3s2/3/3s2	256 × 256	BN	SiLU
halonet50ts	CNN	Yes	3s2/3/3	256 × 256	BN	SiLU
hrnet_w64	CNN	Yes	3s2/3s2	224 × 224	BN	ReLU
lambda_resnet50ts	CNN	Yes	3s2/3/3	256 × 256	BN	SiLU
lamhalobotnet50ts_256	CNN	Yes	3s2/3/3s2	256 × 256	BN	SiLU
nf_resnet50	CNN	Yes	7s2	256 × 256	Norm-free	ReLU
nfnet_l0	CNN	Yes	3s2/3/3s2	224 × 224	Norm-free	ReLU + SiLU
poolformer_m48	CNN	Yes	7s4	224 × 224	GN	GeLU
resnest50d	CNN	Yes	3s2/3/3	224 × 224	BN	ReLU
resnet101	CNN	Yes	7s2	224 × 224	BN	ReLU
resnet50	CNN	Yes	7s2	224 × 224	BN	ReLU
resnet50_gn	CNN	Yes	7s2	224 × 224	GN	ReLU
resnetblur50	CNN	Yes	7s2	224 × 224	BN	ReLU
resnetv2_101	CNN	Yes	7s2	224 × 224	BN	ReLU
resnetv2_50	CNN	Yes	7s2	224 × 224	BN	ReLU
resnetv2_50d_evos	CNN	Yes	3s2/3/3	224 × 224	EvoNorm	-
resnext50_32x4d	CNN	Yes	7s2	224 × 224	BN	ReLU
sebotnet33ts_256	CNN	Yes	3s2/3/3s2	256 × 256	BN	ReLU + SiLU
sehalonet33ts	CNN	Yes	3s2/3/3s2	256 × 256	BN	ReLU + SiLU
seresnet50	CNN	Yes	7s2	224 × 224	BN	ReLU
seresnext50_32x4d	CNN	Yes	7s2	224 × 224	BN	ReLU
wide_resnet50_2	CNN	Yes	7s2	224 × 224	BN	ReLU
convit_base	Transformer	No	16s16	224 × 224	LN	GeLU
crossvit_base_240	Transformer	Yes	16s16	240 × 240	LN	GeLU
deit_base_patch16_224	Transformer	No	16s16	224 × 224	LN	GeLU
deit_small_patch16_224	Transformer	No	16s16	224 × 224	LN	GeLU
jx_nest_tiny	Transformer	Yes	4s4	224 × 224	LN	GeLU
pit_s_224	Transformer	Yes	16s8	224 × 224	LN	GeLU
swin_tiny_patch4_window7_224	Transformer	Yes	4s4	224 × 224	LN	GeLU
tnt_s_patch16_224	Transformer	Yes	7s4	224 × 224	LN	GeLU
vit_base_patch32_224	Transformer	No	32s32	224 × 224	LN	GeLU
vit_small_patch16_224	Transformer	No	16s16	224 × 224	LN	GeLU
gmlp_s16_224	MLP-Mixer	Yes	16s16	224 × 224	LN	GeLU
resmlp_24_224	MLP-Mixer	No	16s16	224 × 224	Affine transform	GeLU
resmlp_big_24_224	MLP-Mixer	Yes	8s8	224 × 224	Affine transform	GeLU
swin_s3_tiny_224	NAS (TFM)	Yes	4s4	224 × 224	LN	GeLU
efficientnet_b2	NAS (CNN)	Yes	3s2	256 × 256	BN	SiLU
fbnetv3_g	NAS (CNN)	Yes	3s2	240 × 240	BN	HardSwish
haloregnetz_b	NAS (CNN)	Yes	3s2	224 × 224	BN	ReLU + SiLU
mixnet_xl	NAS (CNN)	Yes	3s2	224 × 224	BN	ReLU + SiLU
nf_regnet_b1	NAS (CNN)	Yes	3s2	256 × 256	Norm-free	ReLU + SiLU
regnetx_320	NAS (CNN)	Yes	3s2	224 × 224	BN	ReLU
regnety_032	NAS (CNN)	Yes	3s2	224 × 224	BN	ReLU
rexnet_150	NAS (CNN)	Yes	3s2	224 × 224	BN	ReLU + SiLU + ReLU6
coat_lite_small	Hybrid	Yes	4s4	224 × 224	LN	GeLU
pit_b_224	Hybrid	Yes	14s7	224 × 224	LN	GeLU
twins_pepvt_base	Hybrid	Yes	4s4	224 × 224	LN	GeLU
twins_svt_small	Hybrid	Yes	4s4	224 × 224	LN	GeLU
visformer_small	Hybrid	Yes	7s2	224 × 224	BN	GeLU + ReLU
vit_small_r26_s32_224	Hybrid	No	7s2	224 × 224	LN + GN	GeLU + ReLU
xcit_medium_24_p16_224	Hybrid	No	3s2/3s2/3s2/3s2	224 × 224	LN + BN	GeLU
xcit_tiny_12_p8_224	Hybrid	No	3s2/3s2/3s2	224 × 224	LN + BN	GeLU

Table A.3: Description of features of 69 models. “Pooling (stem)” and “Pooling (final)” denote “Pooling at the stem” and “Pooling for final feature”, respectively. “SA”, “CW”, and “DW” means “Self-attention”, “Channel-wise”, and “Depth-wise”, respectively.

Model name	Pooling (stem)	Pooling (final)	2D SA	CW attention	Location of CW attention	DW conv	Group conv
botnet26t_256	Yes	GAP	Yes (BoT)	No		No	No
convmixer_1536_20	No	GAP	No	No		Yes	No
convnext_tiny	No	GAP	No	No		Yes	No
csdarknet53	No	GAP	No	No		No	No
csresnet50	Yes	GAP	No	No		No	No
csresnext50	Yes	GAP	No	No		No	Yes
dla102x2	No	GAP	No	No		No	Yes
dpn107	Yes	GAP	No	No		No	Yes
eca_botnext26ts_256	Yes	GAP	Yes (BoT)	Yes (ECA)	Middle	No	Yes
eca_halonext26ts	Yes	GAP	Yes (Halo)	Yes (ECA)	Middle	No	Yes
eca_nfnet_l0	No	GAP	No	Yes (ECA)	End	No	Yes
eca_resnet33ts	No	GAP	No	Yes (ECA)	Middle	No	No
ese_vovnet39b	No	GAP	No	Yes (ESE)	End	No	No
gcrsnet50t	No	GAP	No	Yes (GCA)	Middle	Yes	No
gcrsnext50ts	Yes	GAP	No	Yes (GCA)	Middle	Yes	Yes
gluon_resnet101_v1c	Yes	GAP	No	No		No	No
gluon_xception65	No	GAP	No	No		Yes	No
halo2botnet50ts_256	No	GAP	Yes (Halo, BoT)	No		No	No
halonet50ts	Yes	GAP	Yes (Halo)	No		No	No
hmet_w64	No	GAP	No	No		No	No
lambda_resnet50ts	Yes	GAP	Yes (Lambda)	No		No	No
lamhalobotnet50ts_256	No	GAP	Yes (Lambda, Halo, BoT)	No		No	No
nf_resnet50	Yes	GAP	No	No		No	No
nfnet_l0	No	GAP	No	Yes (SE)	End	No	Yes
poolformer_m48	No	GAP	No	No		No	No
resnest50d	Yes	GAP	No	Yes		No	Yes
resnet101	Yes	GAP	No	No		No	No
resnet50	Yes	GAP	No	No		No	No
resnet50_gn	Yes	GAP	No	No		No	No
resnetblur50	Yes	GAP	No	No		No	No
resnetv2_101	Yes	GAP	No	No		No	No
resnetv2_50	Yes	GAP	No	No		No	No
resnetv2_50d_evos	Yes	GAP	No	No		No	No
resnext50_32x4d	Yes	GAP	No	No		No	Yes
sebotnet33ts_256	No	GAP	Yes (BoT)	Yes (SE)	Middle	No	No
sehalonet33ts	No	GAP	Yes (Halo)	Yes (SE)	Middle	No	No
seresnet50	Yes	GAP	No	Yes (SE)	End	No	No
seresnext50_32x4d	Yes	GAP	No	Yes (SE)	End	No	Yes
wide_resnet50_2	Yes	GAP	No	No		No	No
convvit_base	No	CLS token	No	No		No	No
crossvit_base_240	No	CLS token	No	No		No	No
deit_base_patch16_224	No	CLS token	No	No		No	No
deit_small_patch16_224	No	CLS token	No	No		No	No
jx_nest_tiny	No	GAP	No	No		No	No
pit_s_224	No	CLS token	No	No		Yes	No
swin_tiny_patch4_window7_224	No	GAP	No	No		No	No
tnt_s_patch16_224	No	CLS token	No	No		No	No
vit_base_patch32_224	No	CLS token	No	No		No	No
vit_small_patch16_224	No	CLS token	No	No		No	No
gmlp_s16_224	No	GAP	No	No		No	No
resmlp_24_224	No	GAP	No	No		No	No
resmlp_big_24_224	No	GAP	No	No		No	No
swin_s3_tiny_224	No	GAP	No	No		No	No
efficientnet_b2	No	GAP	No	Yes (SE)	Middle	Yes	No
fbnetv3_g	No	GAP	No	Yes (SE)	Middle	Yes	No
haloregnetz_b	No	GAP	Yes (Halo)	Yes (SE)	Middle	No	Yes
mixnet_xl	No	GAP	No	Yes (SE)	Middle	Yes	No
nf_regnet_b1	No	GAP	No	Yes (SE)	Middle	Yes	Yes
regnetx_320	No	GAP	No	No		No	Yes
regnety_032	No	GAP	No	Yes (SE)	Middle	No	Yes
rexnet_150	No	GAP	No	Yes (SE)	Middle	Yes	No
coat_lite_small	No	CLS token	No	No		Yes	No
pit_b_224	No	CLS token	No	No		Yes	No
twins_pcpvt_base	No	GAP	No	No		Yes	No
twins_svt_small	No	GAP	No	No		Yes	No
visformer_small	No	GAP	No	No		No	Yes
vit_small_r26_s32_224	Yes	CLS token	No	No		No	No
xcit_medium_24_p16_224	No	CLS token	No	No		Yes	No
xcit_tiny_12_p8_224	No	CLS token	No	No		Yes	No

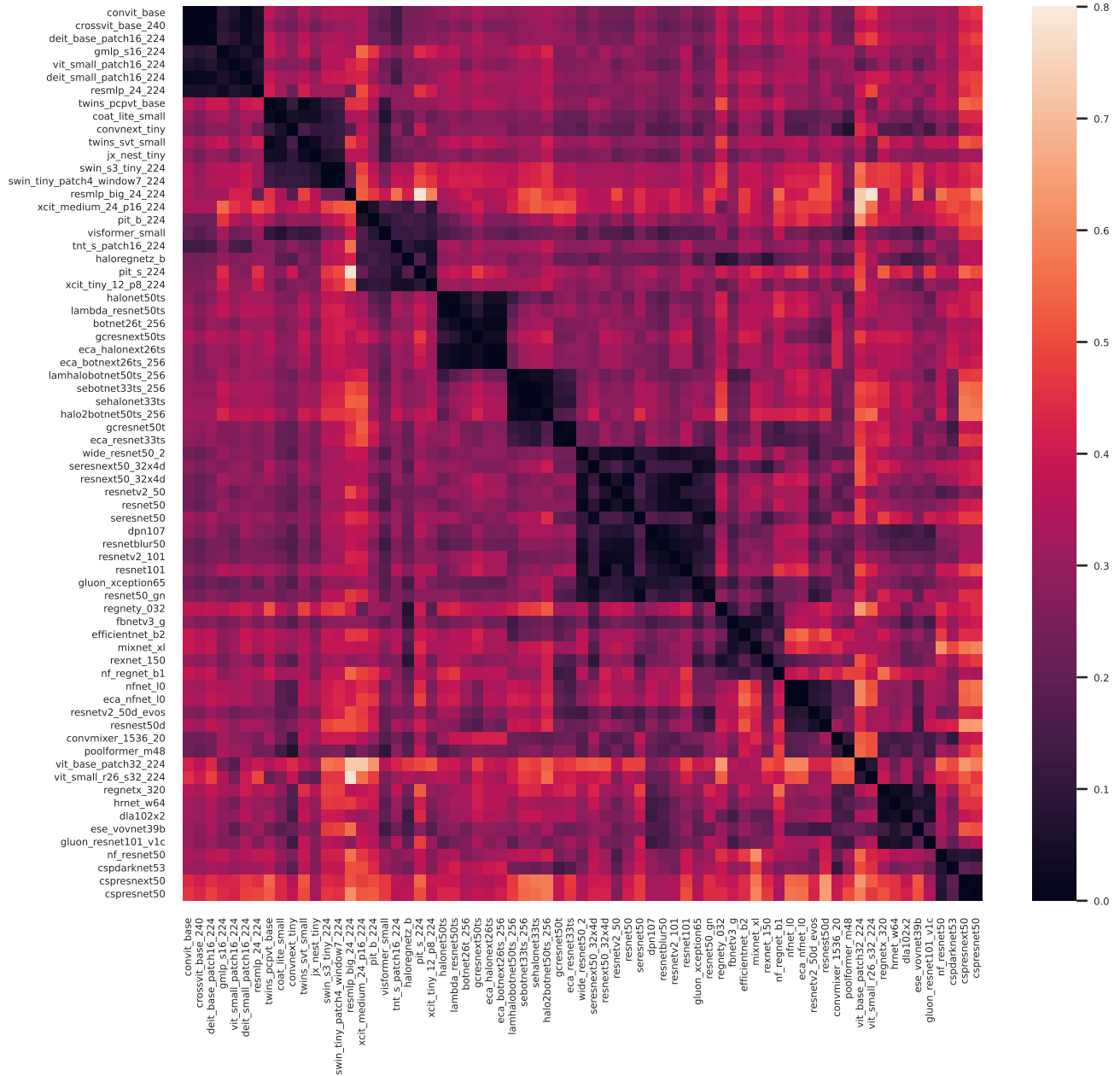


Figure B.1: **Spectral features of 69 architectures.** The K -th largest eigenvectors of the Laplacian matrix of the pairwise similarity graph of 69 architectures are shown ($K = 10$ in this figure). Rows and columns are sorted by the clustering index in Tab. 3 of the main paper. We denote the model name in `timm` for each row and column.

B. Spectral clustering details

We use the normalized Laplacian matrix to compute the Laplacian matrix. We also run K-means clustering 100 times and choose the clustering result with the best final objective function to reduce the randomness by the K-means clustering algorithm.

We visualize the pairwise distances of the spectral features (*i.e.*, K -largest eigenvectors of L) of 69 architectures with their model names in Fig. B.1. This figure is an extension of Fig. 4(a), now including the model names. Note that rows and columns of Fig. B.1 are sorted by the clustering results. Fig. B.1 shows block diagonal patterns, *i.e.*, in-cluster similarities

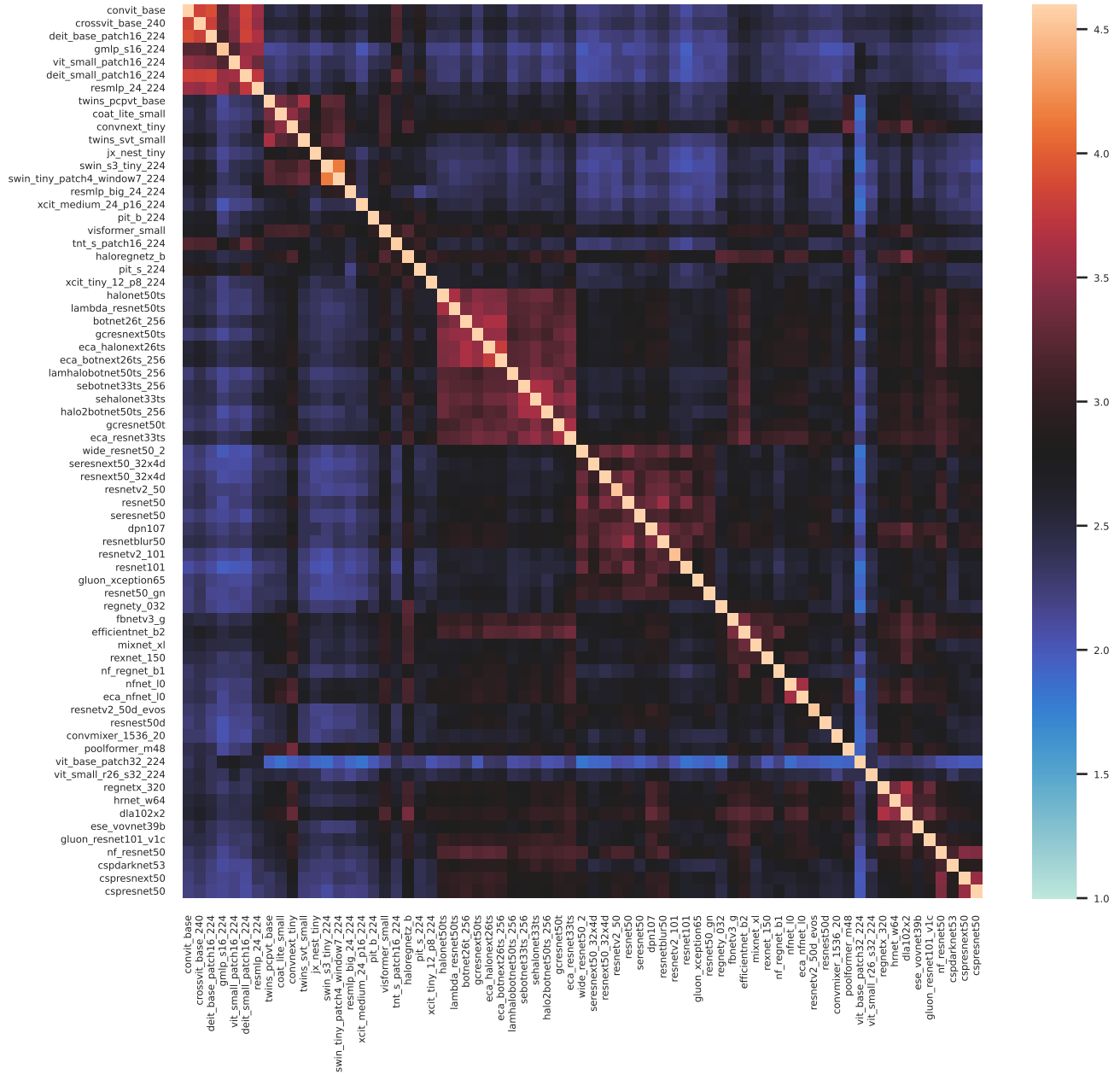


Figure C.1: **Pairwise similarity among 69 models.** Rows and columns are sorted by the clustering index in Tab. 3 of the main paper. (n, n) component of pairwise similarity is close to 4.6 (log 100) because the attack success rate is almost 100% when attacked model and a model used to generate are the same.

are large while between-cluster similarities are small.

C. Pairwise similarities

Fig. C.1 indicates the pairwise similarity among 69 models. We can observe a weak block pattern around clusters, as also revealed in Fig. B.1.

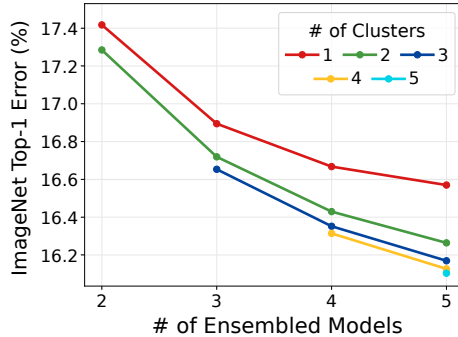


Figure E.1: **Model diversity by architecture difference and ImageNet top-1 error ensemble performance.** We report ImageNet top-1 error by varying the number of ensembled models (N) and the diversity of the ensembled models. The diversity is controlled by choosing the models from k different clusters (larger k denotes more diversity).

D. Training setting details for Sec. 4.2

We train 21 ResNet-50 models and 16 ViT-S from scratch individually by initializing each network with different random seeds. We further train 28 ResNet-50 models by randomly choosing learning rate ($\times 0.1$, $\times 0.2$, $\times 0.5$, $\times 1$, $\times 2$, and $\times 5$ where the base learning rate is 0.1), weight decay ($\times 0.1$, $\times 0.2$, $\times 0.5$, $\times 1$, $\times 2$, and $\times 5$ where the base weight decay is $1e-4$), and learning rate scheduler (step decay or cosine decay). Similarly, we train 9 ViT-S models by randomly choosing learning rate ($\times 0.2$, $\times 0.4$, and $\times 1$ where the base learning rate is $5e-4$) and weight decay ($\times 0.2$, $\times 0.4$, and $\times 1$ where the base weight decay is 0.05). Note that the DeiT training is unstable when we use a larger learning rate or weight decay than the base values. Finally, we collect 22 ResNet-50 models with different training regimes: 1 model with standard training by PyTorch [67]; 4 models trained by GluonCV [35]²; a semi-supervised model and semi-weakly supervised model on billion-scale unlabeled images by Yalniz *et al.* [103]³; 5 models trained by different augmentation methods (Cutout [24], Mixup [109], manifold Mixup [95], CutMix [106], and feature CutMix⁴); 10 optimized ResNet models by [100]⁵. We also collect 7 ViT-S models with different training regimes, including the original ViT training setup [26]⁶, a stronger data augmentation setup in the DeiT paper [89]-3⁶, the training setup with distillation [89]-3⁶, an improved DeiT training setup [90]-3⁶, and self-supervised training fashions by MoCo v3 [12]⁷, MAE [38]⁸ and BYOL [33]⁹. We do not use adversarially-trained networks because the adversarial training usually drops the standard accuracy significantly [92].

E. Ensemble performance

Fig. E.1 shows the ensemble performance by ImageNet top-1 error (lower is better). It has the same tendency as the error reduction rate reported in Fig. 6 of the main paper.

F. Knowledge distillation

F.1. Training setting details for Sec. 5.2

We train ViT-Ti student models with 25 different teacher models using hard distillation strategy. We follow the distillation training setting of DeiT official repo¹⁰, only changing the teacher model. Note that we resize the input images to the input size the teacher model requires if the input sizes of student and teacher models differ. If a teacher model needs a different input resolution, such as 240×240 and 256×256 , we resize the input image for distilling it. Because DeiT-Ti has low classification accuracy compared to teacher models, the similarity score is calculated between DeiT-S and 25

²gluon_resnet50_v1b, gluon_resnet50_v1c, gluon_resnet50_v1d, and gluon_resnet50_v1s from `timm` library.

³ssl_resnet50 and sswl_resnet50 from `timm` library.

⁴We use the official weights provided by <https://github.com/clovaai/CutMix-PyTorch>.

⁵We use the official weights provided by <https://github.com/rwightman/pytorch-image-models/releases/tag/v0.1-rsb-weights>

⁶deit_small_patch16_224, vit_small_patch16_224, deit_small_distilled_patch16_224, and deit3_small_patch16_224 from `timm` library.

⁷We train the ViT-S model by following <https://github.com/facebookresearch/moco-v3>

⁸We train the ViT-S model by following <https://github.com/facebookresearch/mae>

⁹We train the ViT-S model by following <https://github.com/lucidrains/byol-pytorch>

¹⁰<https://github.com/facebookresearch/deit>.

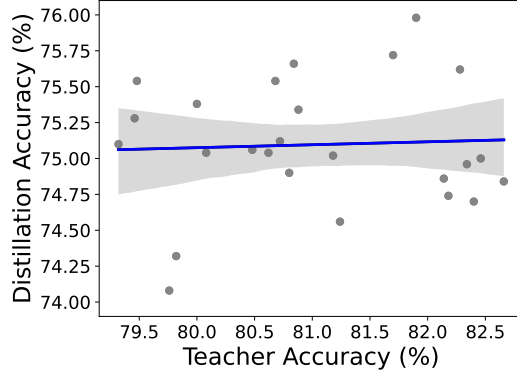


Figure F.1: **Teacher network accuracy and distillation performance.** The trend line and its 90% confidence interval are shown in the blue line and gray band. There is no significant correlation between teacher accuracy and distillation performance.

models. The 25 teacher models are as follows: BoTNet-26, CoaT-Lite Small, ConViT-B, ConvNeXt-B, CrossViT-B, CSPDarkNet-53, CSPResNeXt-50, DLA-X-102, DPN-107, EfficientNet-B2, FBNetV3-G, GC-ResNet-50, gMLP-S, HaloRegNetZ, MixNet-XL, NFNet-L0, PiT-S, RegNetY-032, ResMLP-24, ResNet-50, SEHaloNet33, Swin-T, TNT-S, VisFormer-S, and XCiT-T12.

F.2. Teacher accuracy and distillation performance

The similarity between teacher and student networks may not be the only factor contributing to distillation. For example, a stronger teacher can lead to better distillation performance [107]. In Fig. F.1, we observe that if the range of the teacher accuracy is not significantly large enough (e.g., between 79.5 and 82.5), then the correlation between teacher network accuracy and distillation performance is not significant; 0.049 Pearson correlation coefficient with 0.82 p-value. In this case, we can conclude that the teacher and student networks similarity contributes more to the distillation performance than the teacher performance.

G. Limitations and discussions

Robustness to the choice of adversarial attack methods. Our similarity score is based on attack transferability using the representative gradient-based attack method, PGD attack [61]. To explore the effect of the choice of attack methods, we compute similarity scores on two different gradient-based attack methods; Autoattack [21], which is the state-of-the-art method attack method based on the ensemble of four diverse attacks, and Patchfool attack [29], which is specially designed for vision transformers. We sample 8 models among 69 models for testing the effect of Autoattack on the similarity score: ViT-S, CoaT-Lite Small, ResNet-101, LamHaloBotNet50, ReXNet-150, NFNet-L0, Swin-T and Twins-ppvt. Fig. G.1a shows the high correlation between similarity scores using PGD and Autoattack; it shows a correlation coefficient of 0.98 with a p-value of 1.43×10^{-18} . For testing the Patchfool attack, we only generate adversarial perturbations on ViT-S and get attack transferability to all other models (68 models) because Patchfool targets transformer-based models. In the results, Patchfool also shows a high correlation compared to the PGD attack (Pearson correlation coefficient 0.91 with p-value 3.62×10^{-27}). The results show that our similarity score is robust to the choice of adversarial attack methods if the attack is strong enough. Note that PatchFool needs a heavy modification on the model code to extract attention layer outputs manually. On the other hand, PGD and AutoAttack are model-agnostic and need no modification on the model code. Therefore, if the PatchFool attack and the PGD attack show almost similar similarity rankings, we would like to recommend using PGD because it is easier to use for any architecture.

Similarity scores for adversarially trained networks. Because our method is based on an adversarial attack, it could be affected by an adversarial attack-aware learning method. We first note that our analysis is invariant to the adversarial training; as shown by Tsipras *et al.* [92], adversarial robustness and accuracy are in a trade-off, and there is no ImageNet model with accuracy aligned with our target models yet. Also, our model similarity is based on the difference in the change of the model predictions. As shown by Tsipras *et al.* [92] and Ilyas *et al.* [45], adversarial training will lead to a different decision boundary. Therefore, we think that although our score can be affected by adversarial training, our score is still valid

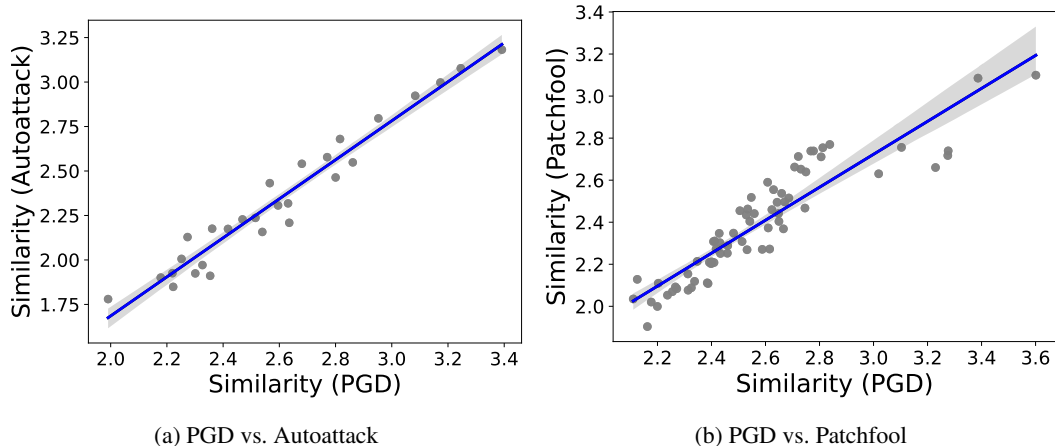


Figure G.1: **Effect of different adversarial attack methods to similarity score.** The trend line and its 90% confidence interval are shown in the blue line and gray band. We show the relationship between our similarity scores using PGD and other attacks, (a) Autoattack and (b) Patchfool attack.

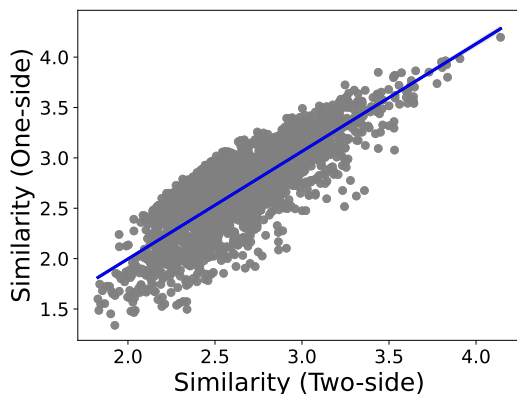


Figure G.2: **Similarity scores using two-side attack transferability vs. one-side attack transferability.** The trend line and its 90% confidence interval are shown in the blue line and gray band. We show the relationship between similarity scores using two-side and one-side attack transferability.

for adversarially trained models because an adversarially trained model is actually dissimilar to other models in terms of the decision boundary and representation learning.

An efficient approximation for a new model. We can use our toolbox for designing a new model; we can measure the similarity between a novel network and existing N architectures; a novel network can be assigned to clusters (Tab. 3 of the main paper) to understand how it works. However, it requires generating adversarial samples for all $N+1$ models (*e.g.*, 70 in our case), which is computationally inefficient. Instead, we propose the approximation of Eq. (1) of the main paper by omitting to compute the accuracy of the novel network on the adversarial samples of the existing networks. It will break the symmetry of our score, but we found that the approximated score and the original score have high similarity (0.82 Pearson correlation coefficient with almost 0 p-value) as shown in Fig. G.2).

As an example, we tested `Gluon-ResNeXt-50` [35], which has the same architecture with `ResNeXt-50` [102] in 69 models, and the distilled version of `DeiT-S` model [89]. Because the difference is not significant as we observed in Tab. 4 and Fig. 4 (b) of the main paper, we expect that `Gluon-ResNeXt-50` is assigned to the same cluster with `ResNeXt-50`, and distilled `DeiT-S` is assigned to the same cluster with `DeiT-S`. We observe that, as we expected, each network is assigned to the desired cluster. Therefore, we suggest using our efficient approximation for analyzing a novel network with our analysis toolbox.

Other possible applications. We can use our similarity to develop a novel neural architecture or training technique by measuring how the proposed method can learn different representations compared to existing methods. Our similarity also can be used for analyzing the hyper-parameter sensitivity. Instead of reporting the performance changes by different hyper-parameters, one can report the average similarity of the trained models with different hyper-parameters. If the average similarity is significantly low, then we can argue that the method is sensitive to hyper-parameter selection. We expect this scenario is especially useful for the task, sensitive to the hyper-parameter selection [15, 34]. Finally, our similarity can be used for the model selection criteria for selecting diverse models, *e.g.*, constructing a new dataset with diverse pre-trained models for annotation candidates [18, 54].